Ruthenium Arene Complexes with Triphenylphosphane Ligands: Cytotoxic Activity Towards Pancreatic Cancer Cells, Interaction with Model Proteins, and Critical Effect of Ethacrynic Acid Substitution

Lorenzo Biancalana,[a] *Alessandro Pratesi,*[b] *Federica Chiellini,*[a] *Stefano Zacchini,*[c] *Tiziana Funaioli,*[a,*] *Chiara Gabbiani,*[a,*] *Fabio Marchetti,*[a,*]

[a] Dipartimento di Chimica e Chimica Industriale, Università di Pisa, Via G. Moruzzi 13, I-56124 Pisa, Italy.

[b] MetMed, Dipartimento di Chimica "Ugo Schiff", Università di Firenze, Via della Lastruccia 3, I-50019 Sesto Fiorentino, Italy.

[c] Dipartimento di Chimica Industriale "Toso Montanari", Università di Bologna, Viale Risorgimento 4, I-40136 Bologna, Italy.

Corresponding Authors

*E-mail addresses: fabio.marchetti1974@unipi.it; tiziana.funaioli@unipi.it; chiara.gabbiani@unipi.it.

Abstract

The ruthenium-arene complexes [(η^6-*p*-cymene)$RuCl_2$(κP-PPh_2(4-$C_6H_4CO_2H$))], **1**, [(η^6-*p*-cymene)RuCl($\kappa^2 P,O$-PPh_2(2-$C_6H_4CO_2$))], **2**, [(η^6-*p*-cymene)$RuCl_2$(κP-PPh_2(2-C_6H_4OCO-EA))], **3**, and [(η^6-*p*-cymene)$RuCl_2$(κP-PPh_2(4-$C_6H_4CO_2CH_2CH_2$OCO-EA))], **4** (EA-CO_2H = ethacrynic acid), were synthesized in good to high yields and characterized by analytical techniques, IR, UV-Vis and multinuclear NMR spectroscopy, and single crystal X-ray diffraction in the cases of **1** and **2**. The unstable compounds [(η^6-arene)$RuCl_2$(κP-PPh_2(2-$C_6H_4CO_2CH_2CH_2$OCO-EA))] (arene = *p*-cymene, **5a**; arene = C_6H_6, **5b**) were obtained and NMR identified in solution. Electrochemical and spectro-electrochemical experiments were performed in order to assess the redox behaviour of **1**-**4** in CH_2Cl_2. The *in vitro* cytotoxicity of **1-4** was determined on the human pancreatic cancer cell line BxPC3 and the mouse embryo fibroblasts Balb/3T3 Clone A31 cell line, the latter acting as a model for normal cells. Furthermore, the interaction of **1**, **3** and **4** with two model proteins was investigated by high resolution ESI-MS.

Keywords: metal-based drugs, ruthenium arene complexes, ethacrynic acid, pancreatic cancer, protein interaction, mass spectrometry.

Introduction

Ruthenium complexes have emerged as promising candidates to overcome the limitations associated with the currently used metal based (platinum based) anticancer drugs, and two of them, *i.e.* [indazoleH][*trans*-Ru(*N*-indazole)$_2Cl_4$] (KP1019) and [imidazoleH][*trans*-Ru(*N*-imidazole)(*S*-DMSO)Cl_4] (NAMI-A), proceeded to the clinical stage of drug development and successfully passed phase I trials (Figure 1).[1] The mechanism of action of these ionic species is believed to involve a single electron reduction process of the Ru(III) centre occurring in the tumour environment.[1,2] Following

these findings, a large variety of ruthenium(II) complexes have been investigated as possible anticancer agents, and especially those complexes based on the [Ru(η^6-arene)Cl_2] scaffold have aroused a considerable interest.[3] Within this family of compounds, RAPTA-C, containing 1,3,5-triaza-7-phosphatricyclo[3.3.1.1]decane (PTA) as a ligand (Figure 1), displays a significant antitumor activity *in vivo* and points towards clinical investigation.[4] In the attempt to modulate the properties of the ruthenium species, several complexes have been prepared by replacement of PTA with a triphenylphosphane derived ligand.[5] Although the lipophilicity of the triphenylphosphane frame may result in a decrease of the water solubility, the introduction of this group usually leads to enhanced cellular uptake and cytotoxicity, possibly favoured by intercalation to DNA.[5b,6]

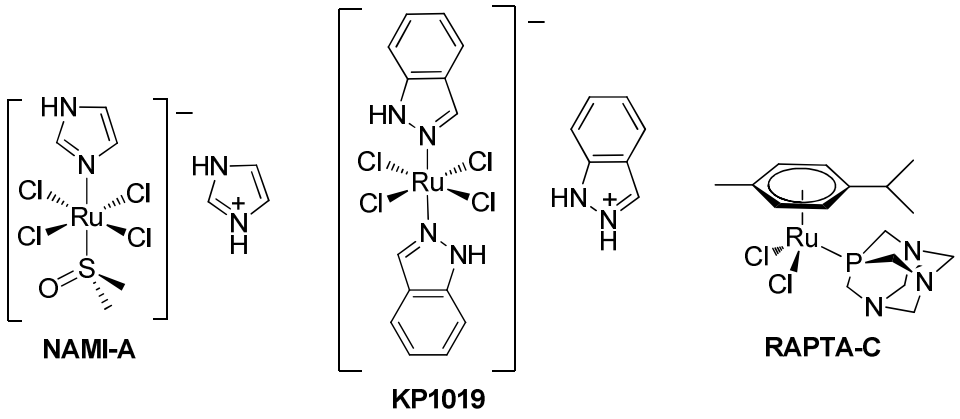

Figure 1. Structures of ruthenium complexes with known antitumor activity.

One of the most common strategies to increase the anticancer activity of metal complexes consists in the inclusion of organic fragments with a known biological function.[2,7] Ethacrynic acid (EA-CO_2H) is a biologically active molecule acting as inhibitor of glutathione transferases (GSTs), i.e. a group of cytosolic detoxification enzymes partially responsible for the drug resistance in primary and metastatic tumours.[8] It has been demonstrated that pancreatic cancer cells display an over-expressed GSTs detoxification system.[9] Ethacrynic acid has been included within ruthenium(II)-arene complexes using

some different synthetic approaches,[8,10] and also platinum(IV) complexes have been modified with ethacrynic acid.[11] The ruthenium compounds have shown the targeted property to inactivate GSTs and determine apoptosis towards ovarian carcinoma, even in the cisplatin resistant cell line.[12]

Only a limited number of ruthenium compounds have been considered as possible drugs against the pancreatic cancer,[13] including Ru(II) arene compounds, and to the best of our knowledge no information regarding triphenylphosphane derivatives have appeared in the literature so far.[3e,14] It should be remarked that the research pointing to new, effective drugs against pancreatic cancer, i.e. one of the deadliest cancers in western countries with a low median survival rate, is of great importance.[15] Indeed pancreatic ductal adenocarcinoma (PDAC), accounting for over 90% of pancreatic cancer cases, develops from the exocrine cells of pancreas, and has usually metastasized by the time it is diagnosed; at that stage, only few clinical treatments can be carried out, mostly palliative and determining severe side effects.[16]

Herein, a series of ruthenium(II)-arene complexes containing triphenylphosphane ligands, two of them functionalized with ethacrynic acid, have been synthesized, fully characterized and investigated for their *in vitro* cytotoxic activity towards the human pancreatic cancer cell line BxPC3 and the mouse embryo fibroblast Balb/3T3 Clone A31 cell line. Additional experiments have been carried out to shed some light on the mechanism of action of the compounds, i.e. electrochemical and spectroelectrochemical analyses, stability studies (NMR, UV-Vis, conductivity) in aqueous medium and studies of reactivity with two small proteins, namely hen egg white lysozyme (HEWL) and horse heart cytochrome c (Cyt-c). These two proteins are suitable to ESI-MS analyses [17] due to their size and overall properties, and, thus, are often used as "model proteins" for metalation studies.[18] It should be mentioned that cytochrome c is importantly involved in apoptotic pathways,[19] while lysozyme is relevant in certain defence mechanisms.[20]

Results and discussion

1. Synthesis and characterization of compounds.

The previously reported triphenylphosphane-ethacrynic acid conjugate **L2** was prepared by a modification of the published procedure,[10a,21] while the new ligands $PPh_2(2\text{-}C_6H_4OCO\text{-EA})$, **L1** and $PPh_2(2\text{-}C_6H_4CO_2CH_2CH_2OCO\text{-EA})$, **L3**, were isolated from the condensation of ethacrynic acid (EA-CO_2H) with (2-hydroxyphenyl)diphenylphosphane or EA-$CO_2(CH_2)_2OH$ with 2-(diphenylphosphino)benzoic acid, respectively (Scheme 1). The synthesis and chromatographic purification of **L1** and **L3** required the use of a strictly inert atmosphere, then these air sensitive products were characterized by analytical and spectroscopic techniques.

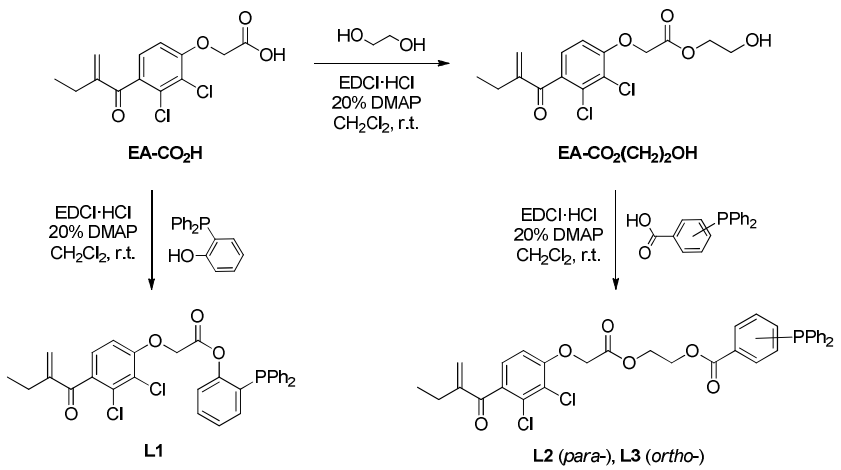

Scheme 1. Synthesis of triphenylphosphane ligands functionalized with ethacrynic acid (EA-CO_2H).

The ruthenium arene complexes **1**-**4** were synthesized by allowing the dimeric precursor $[RuCl_2(p\text{-cymene})]_2$ to react in CH_2Cl_2 or $CHCl_3$ at reflux conditions with an excess of the appropriate phosphane ligand, i.e. $PPh_2(4\text{-}C_6H_4CO_2H)$, $PPh_2(2\text{-}C_6H_4CO_2H)$, **L1** and **L2** respectively (Scheme 2), and then isolated after work up in 65-90% yields. The formation of **2** is accompanied by HCl evolution, leading to bidentate coordination of the resulting phosphino-carboxylate moiety. Compound **2** was alternatively obtained by the reaction of $[RuCl_2(p\text{-cymene})]_2$ with $K[PPh_2(2\text{-}C_6H_4CO_2)]$, affording KCl

as the side product. Complexes **2-3** are unprecedented, whereas **4**,[10a] for which improved synthetic procedure and characterization are given here, and **1** [22] have been already reported.

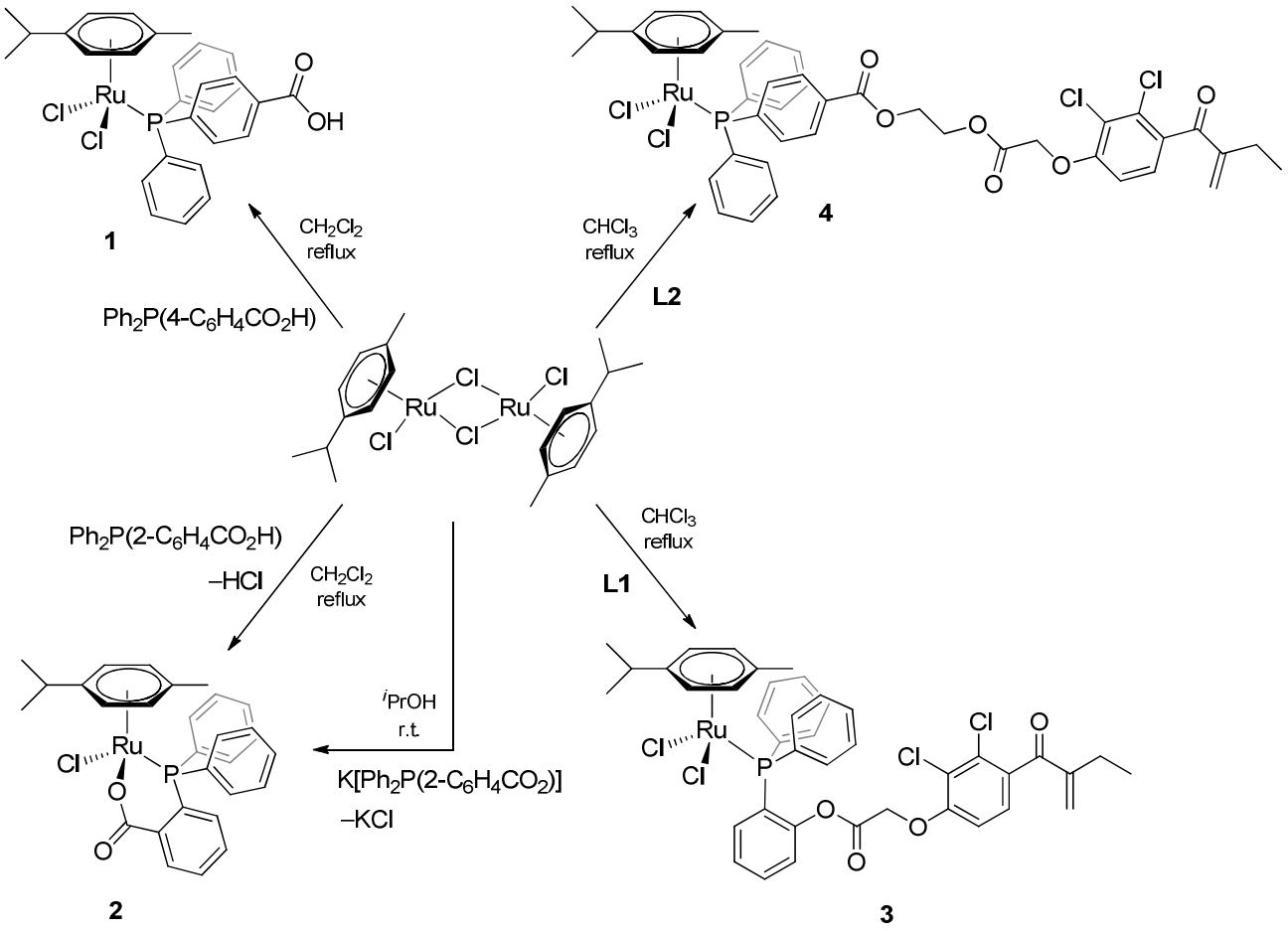

Scheme 2. Synthesis of ruthenium complexes with triphenylphosphane derived ligands.

The reactions of **L3** with $[(arene)RuCl_2]_2$ (arene = *p*-cymene, C_6H_6) proceeded with the initial formation of the expected products **5a-b** (Scheme 3), which were identified in the reaction solution by NMR spectroscopy. However **5a-b** revealed to be unsuitable to biological analyses: an extensive decomposition with release of the arene ligand was observed in the reaction medium, and the compounds were not isolated in the solid state.

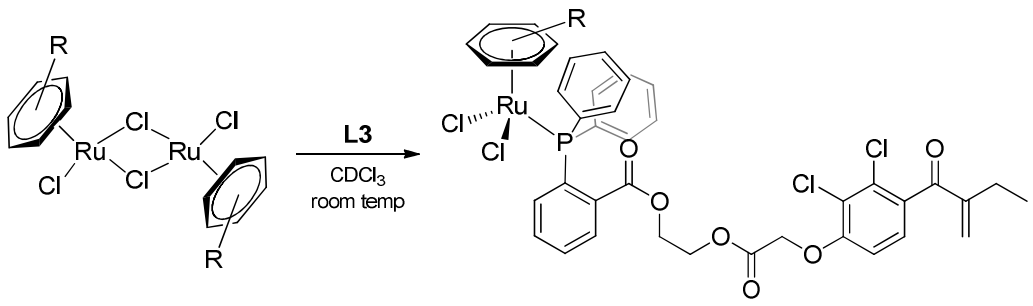

Scheme 3. Formation of unstable Ru(II) phosphane complexes (arene = *p*-cymene, **5a**; C_6H_6, **5b**).

Selected spectroscopic data for **1-5** and related phosphane ligands are compiled in Table S1. The ^{31}P NMR spectra of **1-5** (in $CDCl_3$) consists of one resonance due to the ruthenium bound phosphorous, which is found significantly low field shifted with reference to the corresponding non-coordinated phosphane (*e.g.*, δ = 25.0 ppm in **3** and δ = –16.9 ppm in **L1**). More in detail, the ^{31}P resonance falls at 30.5 ppm in **2**, containing a bidentate *P,O*-ligand, while it occurs around 25 ppm in **1**, **3**, **4** and **5a**, all of these compounds featured by a monodentate phosphane ligand. Complex **2** is a racemate, due to the presence of a stereogenic ruthenium centre, and the two phenyl substituents are diastereotopic. The NMR resonances of the ethacrynic acid fragment in **3-5** [10a,21] and the resonances of the *p*-cymene ligand [10a,23] in **1-4** and **5a** match those previously reported for analogous compounds.

The stable products **1-4** were further characterized by analytical methods and IR and UV-Vis spectroscopy. The IR carbonyl stretching vibration due to the monodentate benzoate group in **2** has been detected at 1604 cm^{-1}, in analogy to the case of a strictly related Ru complex.[24]

X-ray quality crystals of **1** and **2** could be collected from CH_2Cl_2/hexane mixtures settled at 4°C: views of the ORTEP molecular structures are shown in Figures S1 and 2, while relevant bonding parameters are given in Tables S2 and 1, respectively.

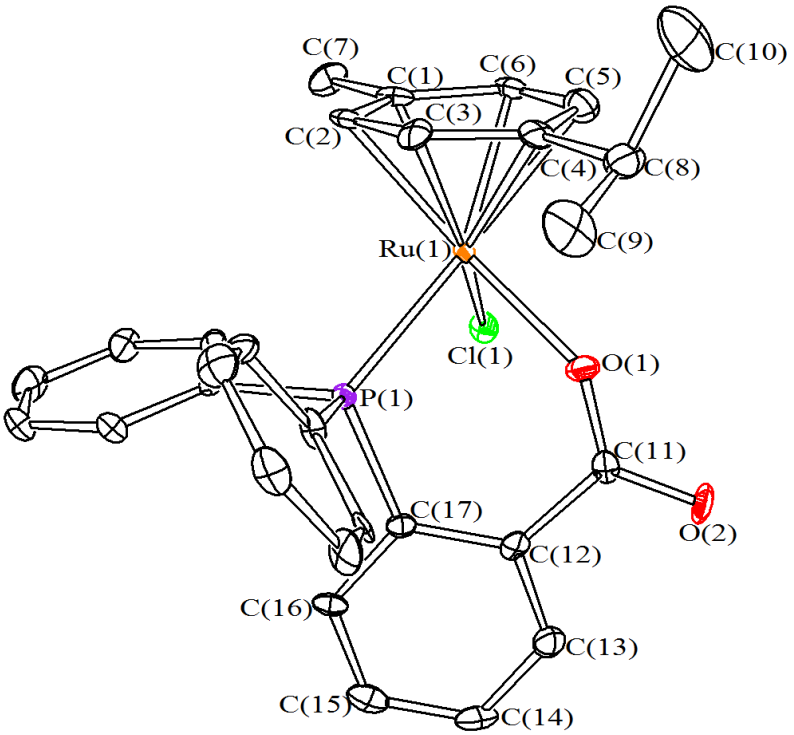

Figure 2. Molecular structure of [(η^6-*p*-cymene)RuCl(κ^2*P,O*-PPh_2(2-$C_6H_4CO_2$))], **2**. Displacement ellipsoids are at the 50% probability level. H-atoms have been omitted for clarity.

Table 1. Selected bond distances (Å) and angles (°) for **2**.

Ru(1)−C(1)	2.219(7)	Ru(1)−C(2)	2.183(7)
Ru(1)−C(3)	2.196(7)	Ru(1)−C(4)	2.191(7)
Ru(1)−C(5)	2.254(8)	Ru(1)−C(6)	2.269(7)
Ru(1)−Cl(1)	2.4197(19)	Ru(1)−O(1)	2.096(5)
Ru(1)−P(1)	2.3168(19)	C(12)−C(11)	1.537(10)
C(11)−O(1)	1.289(9)	C(11)−O(2)	1.235(8)
Cl(1)-Ru(1)−O(1)	87.31(15)	Cl(1)−Ru(1)−P(1)	87.80(7)
O(1)-Ru(1)−P(1)	81.26(15)	C(12)−C(11)−O(1)	121.3(6)
C(12)-C(11)−O(2)	117.2(7)	O(1)−C(11)−O(2)	121.3(7)
Ru(1)-P(1)−C(17)	111.0(2)	P(1)−C(17)−C(12)	121.4(5)

C(17)-C(12)−C(11)	125.1(6)	C(11)−O(1)−Ru(1)	133.5(4)

Compounds **1** and **2** adopt the typical three-leg piano-stool geometry,[25] and the bonding parameters around the Ru(II) centre are similar to those previously reported for related compounds.[10,26] The coordination mode and bonding parameters for the κ^2P,O-$PPh_2(2\text{-}C_6H_4CO_2)$ ligand in **2** are in keeping with previous Ru-complexes displaying the same ligand.[24,27]

2. Electrochemistry and Spectroelectrochemistry.

On considering that the biological activity of ruthenium compounds has been often associated with their involvement in redox processes,[28] the electrochemical behaviour of **1-4**, investigated for their antiproliferative activity (see below), and EA-CO_2H was ascertained by cyclic voltammetry (see Experimental for details). The studied compounds are well soluble in dichloromethane, moreover this solvent offers a wide electrochemical window. The formal electrode potentials for the observed electron transfers are compiled in Table 2, while the CV profiles are shown in Figure 3.

Table 2. Redox properties of **1**-**4** and EA-CO_2H in 0.2 M [^{n}Bu$_4$N][PF$_6$] CH_2Cl_2 solution.

	Oxidation			Reduction		Stability window
	$E^{\circ\prime}$ [a]	ΔE_p [b]	type	E_{pc} [c]	type	ΔE [d]
EA-CO_2H	*none in the solvent window*			-2.14	*irrevers.*	-
1	+1.12	92	*revers.*	-1.81	*irrevers.*	2.93
2	+1.32 [c]	-	*irrevers.*	-1.62	*irrevers.*	2.94
3	+1.15	109	*revers. on CV time-scale*	-1.68	*irrevers.*	2.83
4	+1.11	84	*revers. on CV time-scale*	-1.69	*irrevers.*	2.80

[a] Formal electrode potential (V) *vs.* SCE, calculated as $E^{\circ\prime} = \frac{1}{2}(E_{pa} + E_{pc})$. [b] Peak-to-peak separation (mV) measured at 0.1 $V \cdot s^{-1}$. [c] Peak potential (V) for an irreversible process. [d] Potential difference (V) between oxidation and reduction processes.

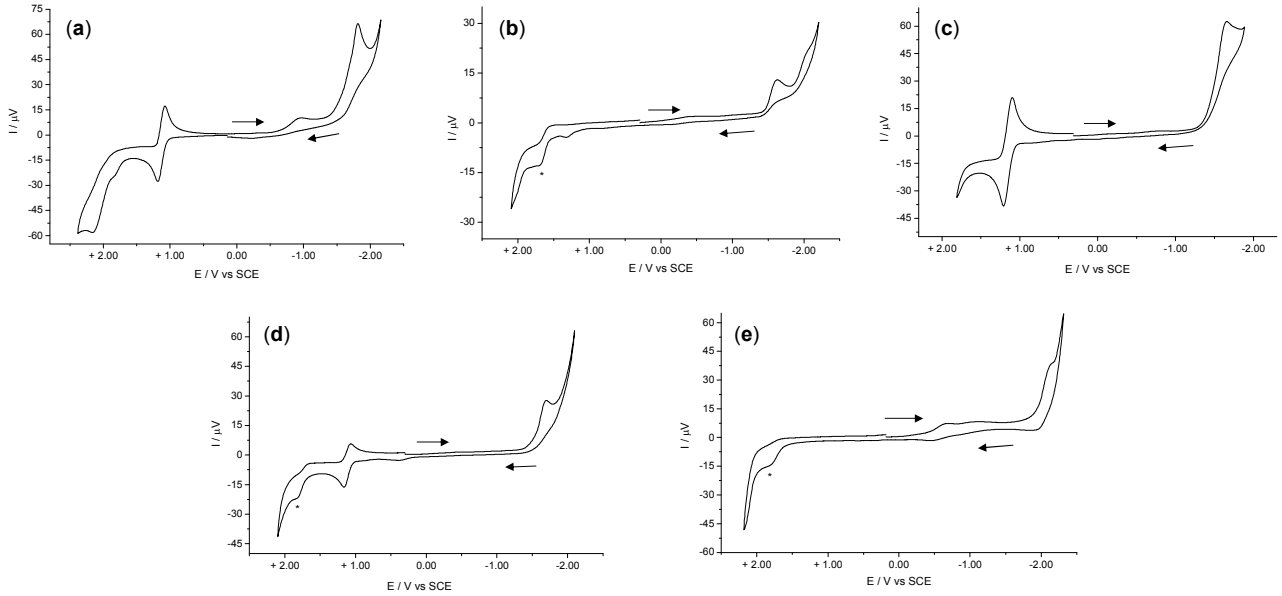

Figure 3. Cyclic voltammograms of **1** (a, $4.1 \cdot 10^{-3}$ M), **2** (b, $6.9 \cdot 10^{-4}$ M), **3** (c, $4.5 \cdot 10^{-3}$ M), **4** (d, $2.6 \cdot 10^{-3}$ M) and EA-CO_2H (e, $2.7 \cdot 10^{-3}$ M) recorded at a Pt electrode in 0.2 M [$^nBu_4N$][PF_6] CH_2Cl_2 solution; scan rate = 0.1 $V \cdot s^{-1}$. The peaks marked with (*) are due to the electrolyte solution. Arrows indicate scan direction.

Ethacrynic acid displayed no oxidation process, while a single irreversible reduction was observed at very low potential (–2.14 V). On the other hand, **1**, **3** and **4** underwent a reversible oxidation process at *ca*. +1.1 V.[29] Similar values were previously reported for related [(η^6-*p*-cymene)$RuCl_2$(PPh_2R)] complexes, containing a monodentate phosphane ligand, and were attributed to a reversible or quasi-reversible $Ru^{2+} \rightarrow Ru^{3+}$ oxidation.[30] Conversely, the *P*,*O* chelate compound **2** showed a weak oxidation wave at +1.32 V, and this process is irreversible even at higher scan rates (up to 1.00 $V \cdot s^{-1}$). The monoelectronic nature of the oxidation process was assessed for **1** as a representative compound, with a combination of controlled-potential coulometry and linear sweep voltammetry (see Experimental for details). In the cathodic region, **1-4** displayed a single irreversible reduction around –1.7 V, electrochemically independent on the Ru^{2+}/Ru^{3+} oxidation discussed above. It was not possible to determine the number of electrons involved in the reduction as the waves occurred at the upper limit of

the potential window provided by the solvent. Concerning related Ru(II)-arene complexes, this process has been assigned to a metal-centred reduction.[30b,31]

The UV-Vis and IR variations related to the electrochemical oxidation of **1**, **3** and **4** were investigated (see Figure S2 given as Supporting Information). Despite the oxidation processes of **3** and **4** are reversible in the CV timescale, the electro-generated species $\mathbf{3}^+$ and $\mathbf{4}^+$ partially decomposed during the longer times required for the macro-electrolysis experiments. Indeed, when the scan rate was reversed some minutes after oxidation was completed, the UV and IR bands became broader and less intense. On the other hand, **1** was cycled several times between positive and negative potentials and no significant change in the UV-Vis and IR spectra was observed. IR carbonyl stretching bands moved to higher wavenumbers on going from the neutral species **1**, **3**, **4** to the corresponding cations (Figure S2 and Table S3). The main variations for the ethacrynic acid-functionalized complexes **3** - **4** are those related to the C=O stretching vibration of the ester group closest to the metal centre: the original bands at 1725 cm^{-1} (**4**) and 1782 cm^{-1} (**3**) were gradually replaced by new bands at 1729 cm^{-1} ($\mathbf{4}^+$) and 1793 cm^{-1} ($\mathbf{3}^+$), respectively. Similarly, the benzoic acid band of **1**, at 1697 cm^{-1}, was replaced on oxidation by an absorption at 1703 cm^{-1}. The removal of one electron from **1**, **3** and **4** produced a markedly different pattern in the respective UV-Vis spectra (Figure S2): more precisely, the 370-375 nm band was replaced by four new bands at 315, 355, 420 and 515 nm.

In conclusion, **1-4** exhibit a comparable electrochemical behaviour, with minor differences imputable to the coordination mode of the phosphane ligand (mono- or bidentate) and the nature of the substituent on the triphenylphosphane frame (carboxylic acid or ester). However, no redox activity has been detected within a biologically relevant range of potentials;[32] therefore, despite these findings refer to dichloromethane solutions, the complexes are reasonably expected not to be engaged in redox processes in physiological environment, and the Ru(II) oxidation state to be preserved.

3. Stability studies.

NMR and UV-Vis spectroscopy and conductivity measurements were used to assess the stability of the complexes **1-4** in DMSO/water 9:1 solutions at 37 °C as a function of time. The high relative content of DMSO in the solvent mixture was required in order to obtain $1 \cdot 10^{-2}$ mol·L^{-1} solutions of Ru compounds, this concentration being suitable for NMR analysis. Parallel NMR and UV-Vis analyses were conducted on **1-4** in 0.11 M sodium chloride DMSO/water solutions. This chloride concentration resembles that present in the medium used for *in vitro* tests, and that typical of blood. The details of the experiments are reported in the SI, and the compounds identified in the distinct cases after 72 h are shown in Scheme 4. Only a fraction, ranging from 45% (**2** and **4**) to 24% (**1** and **3**), of the starting ruthenium complexes was still persistent in solution after 72 h in the absence of NaCl (Table 3). Interestingly, the addition of 0.11 M NaCl significantly suppressed the decomposition of **1-3** (*e.g.* 49% of **3** detected after 72 h), see Table 3, without causing any variation to the ^{1}H and ^{31}P set of signals. Degradation pathways of **1-4** include the dissociation of the phosphane and *p*-cymene ligands. Thus, 4-(diphenylphosphino)benzoic acid, **L1** and **L2** were recognized in significant amounts, in admixture with the respective phosphane-oxides. The NMR data suggest that no hydrolytic cleavage of the ester bonds occurred, *i.e.* the ethacrynic acid fragment is preserved within the relevant phosphane. On the other hand, minor amounts of non coordinated 2-(diphenylphosphino)benzoate (identified as phosphane oxide) was released from **2**. This feature is presumably a consequence of the bidentate coordination providing additional stability to the Ru-P linkage.

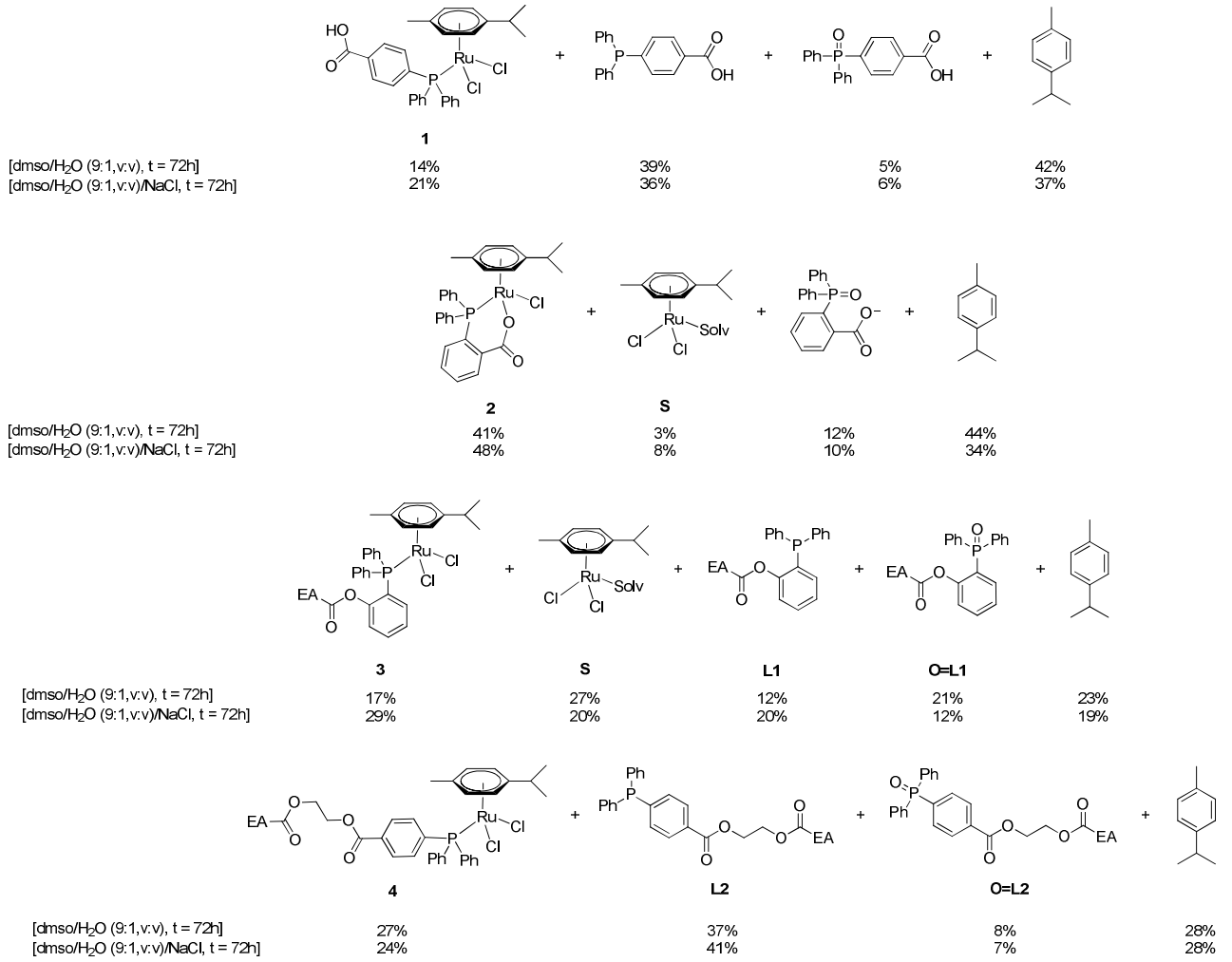

Scheme 4. Compounds detected in DMSO/H_2O and DMSO/H_2O/NaCl solutions of **1-4** maintained at 37 °C; % values are based on ^{1}H NMR spectroscopy and refer to identified compounds only.

Table 3. Fraction of complexes **1-4** in DMSO/H_2O and DMSO/H_2O/NaCl solutions at 37 °C; % values are based on ^{1}H NMR spectroscopy (dimethyl sulfone as internal standard, 1:1 molar ratio vs Ru).

Compound	% (result of NaCl experiment in parenthesis)		
	t = 0	t = 25.5 h	t = 72 h
1	90 (95)	59 (67)	23 (35)
2	96 (97)	72 (71)	45 (52)
3	64 (62)	39 (62)	24 (49)
4	82 (82)	72 (66)	45 (39)

4. Cytotoxicity studies.

The ability to inhibit cell growth of the complexes **1-4**, selected phosphane(oxide) species, ethacrynic acid and the reference compounds RAPTA-C and cisplatin was evaluated *in vitro* against the human pancreatic cancer cell line BxPC3 and the mouse embryo fibroblast Balb/3T3 Clone A31 cell line, the latter representing a model for non-tumour cells. Since the compounds are almost insoluble in water, stock solutions were prepared in DMSO and then diluted with cell culture media.

The obtained IC_{50} values are visualized in Table 4. The ethacrynic acid-functionalized compounds **3** and **4** displayed an enhanced antiproliferative activity with respect to **1** and **2**, and ethacrynic acid itself. Therefore, a synergic effect can be envisaged as obtained by linking ethacrynic acid to the ruthenium arene triphenylphosphane frame. It is plausible that the ethacrynic acid moiety contributes to the anticancer effect via the inhibition of GSTs, which sensitizes the cancer cells towards the ruthenium species; intracellular esterases might be implicated in separating the EA-CO_2H fragment from the ligand/complex, as previously proposed.[12,33]

Compound **1** did not show appreciable cytotoxicity, in agreement with a recent investigation on other cell lines.[22] The IC50 values of $PPh_2(4\text{-}C_6H_4CO_2H)$, $[PPh_2(2\text{-}C_6H_4CO_2)]^-$ (as K^+ salt) and **L1** were found to be lower than the maximum tested concentration, conversely the phosphane oxide **L2=O** exhibited some cytotoxic activity, all of these species being generated from the respective complexes in aqueous medium (see Stability Studies section); likewise **L2=O**, also **L2** is expected to exert a cytotoxic behaviour.[10] On account of the fact that $K[PPh_2(2\text{-}C_6H_4CO_2)]$, **L1** and **L2=O** display significantly higher IC_{50} values compared to the respective complexes **2-4** (see above), it may be assumed that the antiproliferative activity of **2-4** is essentially due to the intact ruthenium-phosphane species.

Compounds **2** and **3** display a moderate selectivity towards the BxPC3 cell line with respect to the non tumoral cell line, and a reverse situation was found for **4**. On comparing the data related to **3** and **4**, it

can be concluded that the site and chemical nature of the binding of the ethacrynic acid moiety to the phosphane ligand (Scheme 2) may play a significant role in the cytotoxic activity of the resulting complexes. The IC_{50} values obtained for **3** appear promising when compared to those obtained for cisplatin on the same cell lines.

Table 4. IC_{50} values (μM) of tested compounds.

Compound	IC_{50} (μM) ± SD	
	BxPC3	Balb/3T3 CloneA31
1	>80	>80
2	31 ± 5	52 ± 3
3	7.7 ± 1.4	14.1 ± 0.3
4	13.4 ± 0.4	8.6 ± 0.5
$PPh_2(4\text{-}C_6H_4CO_2H)$	>80	>80
$K[PPh_2(2\text{-}C_6H_4CO_2)]$	>80	>80
L1	>80	>80
O=L2	34 ± 7	49 ± 8
EA-CO_2H	>80	>80
cisplatin	11.0 ± 0.3	13 ± 2
RAPTA-C	> 500	-

BxPC3 = human pancreatic cancer cell line; Balb/3T3 CloneA31 = mouse embryo fibroblast cell line.

5. Interaction of complexes with model proteins.

To gain a deeper insight into the reactivity of the compounds with potential biomolecular targets, **1**, **3** and **4** were allowed to react with HEWL and Cyt-c. A three fold molar excess of each complex was incubated with the selected protein in an ammonium acetate buffer at 37 °C, and the resulting adducts were analyzed by ESI–MS as a function of time up to 72 h, according to a previously described protocol.[18a] Thus, the interaction of **1**, **3** and **4** with cytochrome c resulted in a fragmentation of the

metal complexes, leading to the formation of the adduct *cyt-Ru-cym* (peak at *m/z* 12592 Da), consisting of cytochrome c added of the Ru(η^6-*p*-cymene) moiety. It is noteworthy that the same adduct was recognized as the prevalent product of the interaction between cytochrome c and other ruthenium arene compounds, including RAPTA-C.[34] However, some differences have been observed within compounds **1**, **3** and **4**. In the case of **1**, the reaction did not reach completion, and the intact protein was detected in a significant amount after 72 h of incubation (Figure 4). Conversely, in the case of **3**, the formation of *cyt-Ru-cym* was almost completed after 24 h, and only a small amount of protein remained unreacted (Figure 5). A further minor peak was assigned to *cyt-Ru-cym* with the addition of ethacrynic acid (*m/z* 12895 Da).

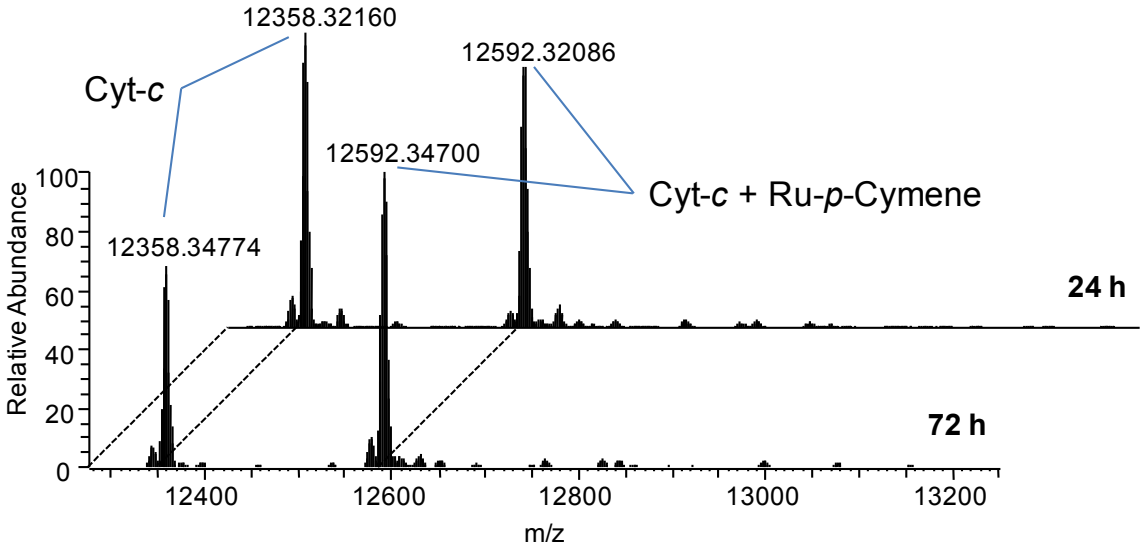

Figure 4. Deconvoluted ESI–MS spectra of cytochrome c in ammonium acetate buffer (pH 6.8), incubated with complex **1**, after 24 and 72 h respectively, at 37 °C (protein concentration = 10^{-4} M; **1**/protein molar ratio = 3).

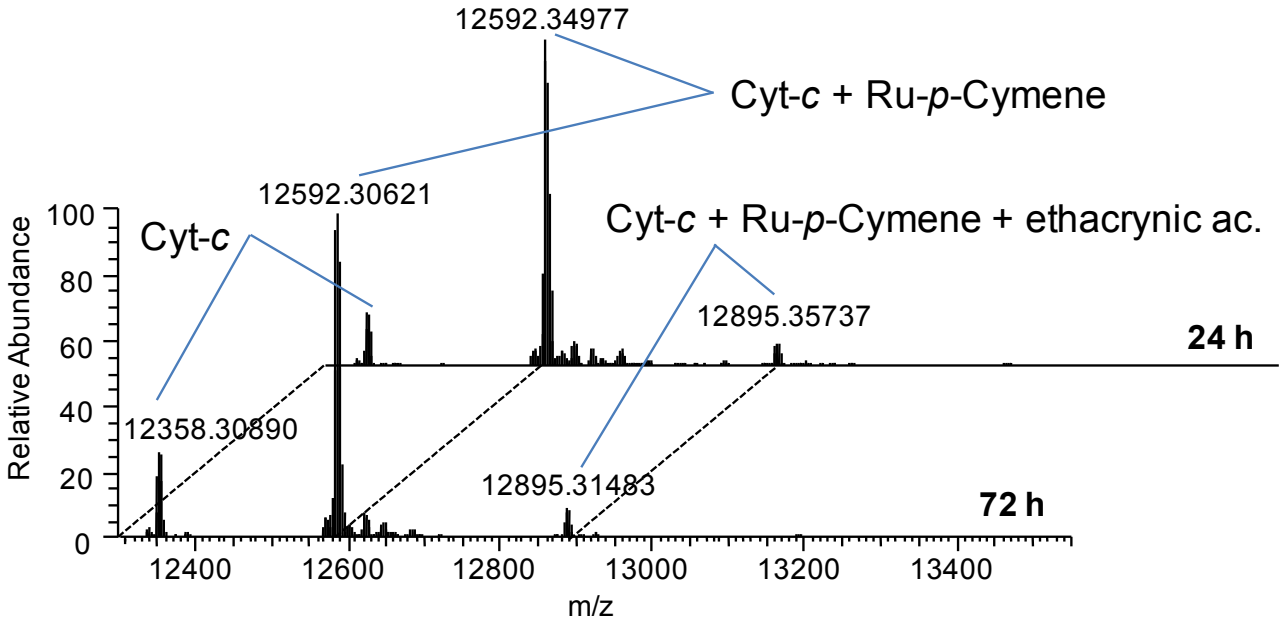

Figure 5. Deconvoluted ESI–MS spectra of cytochrome c in ammonium acetate buffer (pH 6.8), incubated with complex **3**, after 24 and 72 h respectively, at 37 °C (protein concentration = 10^{-4} M; **3**/protein molar ratio = 3).

Also in the case of **4**, the formation of the adduct *cyt-Ru-cym* (see above) occurred with extensive consumption of the ruthenium species, although this process was slower than in the case of **3** (Figure 6). In fact, a significant amount of unreacted protein was still present after 24 h, and a peak attributed to the adduct *cyt-[Ru(DMSO)(H_2O)]* was also detected.

Stability studies in DMSO/water solution have indicated that these Ru complexes undergo a slow dissociation of the phosphane ligand (see Stability Studies section), and this fact may be associated to the possibility of effective binding of the Ru(*p*-cymene) fragment to the protein side chain, as observed in the case of Cyt-c.

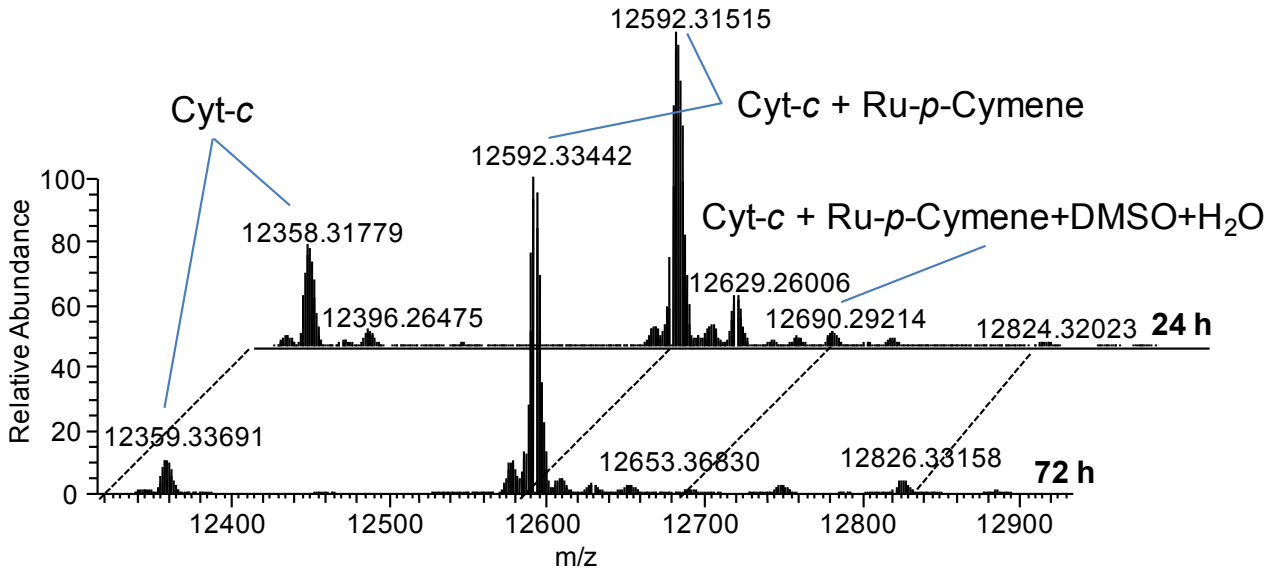

Figure 6. Deconvoluted ESI–MS spectra of cytochrome c in ammonium acetate buffer (pH 6.8), incubated with complex **4**, after 24 and 72 h respectively, at 37 °C (protein concentration = 10^{-4} M; **4**/protein molar ratio = 3).

Additional ESI-MS studies were performed to elucidate the reactivity of **1**, **3** and **4** with lysozyme. A markedly lower reactivity of the complexes was ascertained compared to the analogous reactions with cytochrome c (see Figure S3).

Conclusions

Some ruthenium arene complexes containing different triphenylphosphane ligands have been prepared, structurally characterized and evaluated *in vitro* as possible drugs against pancreatic adenocarcinoma. The incorporation of ethacrynic acid, i.e. a bioactive molecule implicated in resistance mechanisms, via the phosphane ligand has provided a synergic effect enhancing the antiproliferative activity of the complexes. Electrochemical and spectroscopic experiments and ESI-MS studies on the interaction with model proteins have given insight into the behaviour of the complexes in biological environment. The complexes functionalized with ethacrynic acid undergo slow and progressive dissociation of the phosphane ligand, possibly converting into the relevant phosphane oxide, these uncoordinated species providing minor contribution to the cytotoxic activity. The enhanced phosphane release seems to be related to the possibility of effective binding of the ruthenium-arene fragment to a model protein (cytochrome c). It is noteworthy that the stability of the ethacrynic acid functionalized complexes, their anticancer behaviour and the adduct formation with proteins may be tuned by an appropriate, synthetic choice of the site and linkage of the bioactive moiety to the phosphane.

Experimental

$[(\eta^6\text{-}p\text{-cymene})RuCl_2]_2$ and $[(\eta^6\text{-}C_6H_6)RuCl_2]_2$ were prepared according to the literature from $RuCl_3 \cdot xH_2O$ (99.9%, Alfa Aesar) and α-phellandrene or 1,3-cyclohexadiene, respectively (Sigma Aldrich).[35] The other organic reactants were obtained from Alfa Aesar, Sigma Aldrich or TCI Europe and were of the highest purity available. Ethylene glycol, 4-(diphenylphosphino)benzoic acid, 2-(diphenylphosphino)benzoic acid, (2-hydroxyphenyl)diphenylphosphane, ethacrynic acid (EA-CO_2H) and ethyl(diisopropylamino)carboxydiimide hydrochloride (EDCI·HCl) were stored under nitrogen as received. Synthesis of ligands and complexes was carried out under a nitrogen atmosphere using standard Schlenk techniques. Solvents were distilled from appropriate drying agents. Once isolated, **L1**, **L2**, **L3** and $K[PPh_2(2\text{-}C_6H_4CO_2)]$ were stored under nitrogen. Silica gel (Merck, 70-230 mesh) was dried at 150 °C overnight and stored under nitrogen. NMR spectra were recorded at 298 K on a Bruker Avance II DRX400 instrument equipped with a BBFO broadband probe. Chemical shifts (expressed in parts per million) are referenced to the residual solvent peaks (^1H, $^{13}C\{^1H\}$) or to external standard ($^{31}P\{^1H\}$ to 85% H_3PO_4). Spectra were assigned with the assistance of DEPT-135, ^1H-^1H (COSY) and ^1H-^{13}C (*gs*-HSQC and *gs*-HMBC) correlation experiments.[36] Infrared spectra of solid samples were recorded on a Perkin Elmer Spectrum One FT-IR spectrometer, equipped with a UATR sampling accessory. Infrared spectra of liquid samples were recorded on a Perkin Elmer Spectrum 100 FT-IR spectrometer with a CaF_2 liquid transmission cell. UV-Vis spectra were recorded on a Ultraspec 2100 Pro spectrophotometer with 0.1 cm quartz cuvettes. Carbon and hydrogen analysis was performed on a Carlo Erba mod. 1106 instrument. Melting points and decomposition temperatures were determined on a STMP3 Stuart scientific instrument with a capillary apparatus. Conductivity measurements were carried out at 21°C using an XS COND 8 instrument (cell constant = 1.0 cm^{-1}).[37]

1) Synthesis and characterization of compounds.

Synthesis of EA-$CO_2(CH_2)_2OH$.

Chart 1. Structure of EA-$CO_2(CH_2)_2OH$ (numbering refers to carbon atoms).

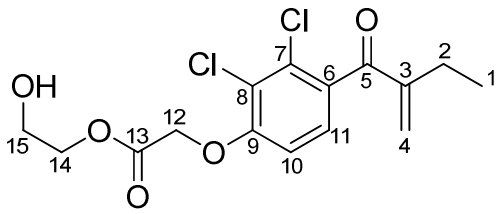

The title compound was prepared according to a modified literature procedure.[10a] A solution of EA-CO_2H (314 mg, 1.03 mmol) and ethylene glycol (0.60 mL, 11 mmol) in THF (8 mL) was treated with EDCI·HCl (235 mg, 1.23 mmol) and DMAP (24 mg, 0.19 mmol). The colourless suspension (oil + solution) was stirred at room temperature and the progress of reaction was monitored with TLC. After 2.5 hours, volatiles were removed under vacuum. The colourless residue was dissolved in CH_2Cl_2 and extracted with water (x 3). The organic phase was concentrated under vacuum and loaded on top of a silica column. Impurities were eluted with CH_2Cl_2, then EA-$CO_2(CH_2)_2OH$ was collected with CH_2Cl_2/Et_2O (1:1 *v*/*v*). Solvent removal under vacuum (room temperature) yielded EA-$CO_2(CH_2)_2OH$ as an air stable, colourless crystalline solid. Yield: 229 mg, 64%. Anal. calcd. for $C_{15}H_{16}Cl_2O_5$: C, 51.89; H, 4.65. Found: C, 51.63; H, 4.71. IR (solid state): $\tilde{\upsilon}/cm^{-1}$ = 3512w ($\nu_{O\text{-}H}$), 3089w, 2976w, 2965w, 2940w, 2921w, 2881w, 1737s ($\nu_{C13=O}$), 1662s ($\nu_{C5=O}$), 1625w, 1587m ($\nu_{C3=C4}$), 1559w, 1472m, 1445m, 1414m, 1383m, 1359m, 1292m, 1258m, 1230s, 1205s, 1124m, 1076s, 1001m, 943m, 892m, 842m, 810m, 769m, 736m. UV-Vis (CH_2Cl_2): λ_{max}/nm ($\varepsilon/M^{-1}\cdot cm^{-1}$) = 267 ($4.8\cdot10^3$). ^{1}H NMR ($CDCl_3$): δ/ppm = 7.14 (d, $^3J_{HH}$ = 8.5 Hz, 1H, C11-H), 6.81 (d, $^3J_{HH}$ = 8.5 Hz, 1H, C10-H), 5.95 (s, 1H, C4-H), 5.61 (s, 1H, C4-H'), 4.82 (s, 2H, C12-H), 4.39–4.33 (m, 2H, C14-H), 3.89–3.84 (m, 2H, C15-H), 2.47 (q, $^3J_{HH}$ = 7.4 Hz, 2H, C2-H), 1.83 (s, 1H, OH), 1.15 (t, $^3J_{HH}$ = 7.4 Hz, 3H, C1-H).

Synthesis of PPh_2(2-C_6H_4OCO-EA), L1.

Chart 2. Structure of PPh_2(2-C_6H_4OCO-EA), **L1** (numbering refers to carbon atoms).

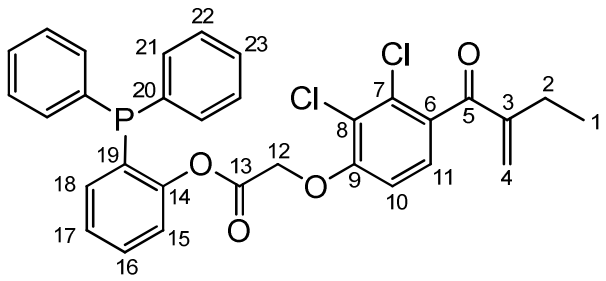

A solution of (2-hydroxyphenyl)diphenylphosphane (206 mg, 0.739 mmol) and EA-CO_2H (247 mg, 0.813 mmol) in CH_2Cl_2 (15 mL) was treated with EDCI·HCl (156 mg, 0.816 mmol) and then with DMAP (20 mg, 0.16 mmol). The resulting colourless solution was stirred at room temperature for 24 hours. Volatiles were removed under vacuum and a colourless foamy solid was obtained. The solid was washed with hexane then suspended in boiling Et_2O (20 mL) for 1 hour. The liquid was filtered and collected into another flask and the extraction procedure was repeated three times. **L1** was obtained as an air sensitive, colourless solid after solvent removal under vacuum. Yield: 358 mg, 86%. Anal. calcd. for $C_{31}H_{25}Cl_2O_4P$: C, 66.09; H, 4.47. Found: C, 66.22; H, 4.38. Mp: 58°C (colourless liquid). IR (solid state): $\tilde{\upsilon}/cm^{-1}$ = 3059w, 2966w, 2933w, 2874w, 1779m ($\nu_{C13=O}$), 1663s ($\nu_{C5=O}$), 1624w-sh, 1584s ($\nu_{C3=C4}$), 1466s, 1435s, 1384m, 1339w, 1292m, 1259s, 1228m, 1219m, 1186m, 1155s, 1118m, 1076s, 1028m-sh, 1000m, 946w, 911w, 802m, 743s, 694s. ^{1}H NMR ($CDCl_3$): δ/ppm = 7.43–7.25 (m, 11H, Ph), 7.24–7.16 (m, 2H, Ph), 7.04 (d, $^3J_{HH}$ = 8.5 Hz, 1H, C11-H), 6.88–6.83 (m, 1H, Ph), 6.66 (d, $^3J_{HH}$ = 8.7 Hz, 1H, C10-H), 5.93 (s, 1H, C4-H), 5.58 (s, 1H, C4-H'), 4.69 (s, 2H, C12-H), 2.47 (q, $^3J_{HH}$ = 7.5 Hz, 2H, C2-H), 1.15 (t, $^3J_{HH}$ = 7.4 Hz, 3H, C1-H). $^{13}C\{^1H\}$ NMR ($CDCl_3$): δ/ppm = 196.0 (C5), 166.1 (C13), 155.5 (C9), 152.2 (d, $^2J_{CP}$ = 14.4 Hz, C14), 150.3 (C3), 135.4 (d, $^2J_{CP}$ = 8.6 Hz, C18), 134.2 (C8), 134.0 (d, $^2J_{CP}$ = 20.5 Hz, C21), 131.5 (C7), 130.4 (C16), 129.4 (C23), 128.9 (d, $^3J_{CP}$ = 6.9 Hz,

C22), 128.7 (C4), 127.0 (C11/C17), 126.9 (C11/C17), 122.4 (C6 + C15), 111.5 (C10), 66.0 (C12), 23.6 (C2), 12.6 (C1). $^{31}P\{^{1}H\}$ NMR ($CDCl_3$): δ/ppm = – 16.9.

Synthesis of PPh_2(4-$C_6H_4CO_2CH_2CH_2OCO$-EA), L2.

Chart 3. Structure of PPh_2(4-$C_6H_4CO_2CH_2CH_2OCO$-EA), **L2** (numbering refers to carbon atoms).

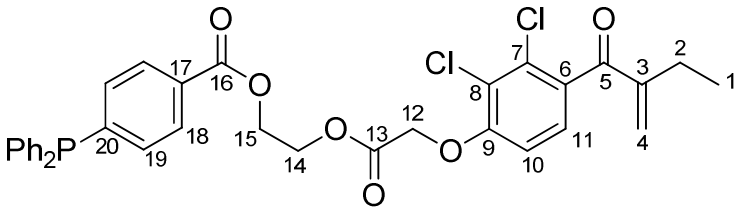

The title compound was prepared according to a modified literature procedure.[10a] A solution of 4-(diphenylphosphino)benzoic acid (131 mg, 0.426 mmol) and EA-$CO_2(CH_2)_2OH$ (124 mg, 0.355 mmol) in CH_2Cl_2 (20 mL) was treated with EDCI·HCl (102 mg, 0.533 mmol) and DMAP (9.2 mg, 0.075 mmol). The resulting pale yellow solution was stirred at room temperature and the progress of the reaction was monitored by TLC. After 6.5 hours, the volume was reduced under vacuum to 2-3 mL, then Et_2O was slowly added. The colourless milky suspension was filtered on a short silica pad and eluted with Et_2O. Volatiles were removed under vacuum and compound **L2** was obtained as an air sensitive, colourless sticky solid. Yield: 178 mg, 79%. Anal. calcd. for $C_{34}H_{29}Cl_2O_6P$: C, 64.26; H, 4.60. Found: C, 64.07; H, 4.65. IR (solid state)[10a]: $\tilde{\upsilon}/cm^{-1}$ = 1763m ($\nu_{C13=O}$), 1718s ($\nu_{C16=O}$), 1665m ($\nu_{C5=O}$), 1584m ($\nu_{C3=C4}$). ^{1}H NMR ($CDCl_3$): δ/ppm = 7.95 (dd, $^{3}J_{HH}$ = 8.4 Hz, $^{4}J_{HP}$ =1.4 Hz, 2H, C18-H), 7.38–7.29 (m, 12H, C19-H + Ph_2P), 7.07 (d, $^{3}J_{HH}$ = 8.5 Hz, 1H, C11-H), 6.79 (d, $^{3}J_{HH}$ = 8.5 Hz, 1H, C10-H), 5.91 (s, 1H, C4-H), 5.56 (s, 1H, C4-H'), 4.78 (s, 2H, C12-H), 4.55 (s, 4H, C14-H + C15-H), 2.46 (q, $^{3}J_{HH}$ = 7.4 Hz, 2H, C2-H), 1.14 (t, $^{3}J_{HH}$ = 7.4 Hz, 3H, C1-H). $^{31}P\{^{1}H\}$ NMR ($CDCl_3$): δ/ppm = – 4.9.

Synthesis of PPh_2(2-$C_6H_4CO_2CH_2CH_2OCO$-EA), L3.

Chart 4. Structure of PPh_2(2-$C_6H_4CO_2CH_2CH_2OCO$-EA), **L3** (numbering refers to carbon atoms).

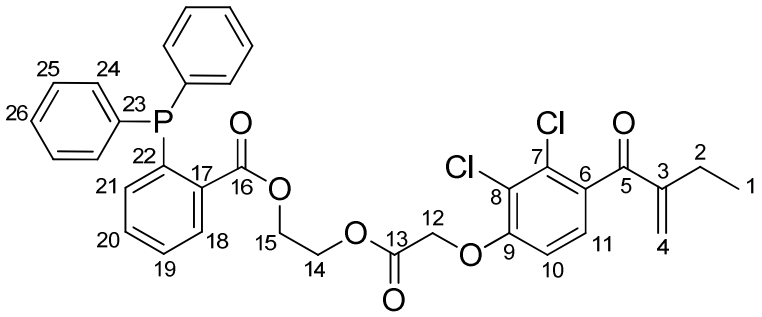

The title compound was prepared as described for **L2**, using 2-(diphenylphosphino)benzoic acid (240 mg, 0.783 mmol), EA-$CO_2(CH_2)_2OH$ (227 mg, 0.564 mmol), EDCI·HCl (188 mg, 0.980 mmol) and DMAP (17 mg, 0.14 mmol). The resulting pale yellow solution was stirred at room temperature and the progress of the reaction was monitored by TLC. After 14 hours, the volume was reduced under vacuum to 2-3 mL, then Et_2O (10 mL) was slowly added. The resulting suspension was loaded on a short silica column (h 2 cm, d 3 cm) equipped with an external glass jacket filled with a NaCl/ice mixture (T = -14°C). Compound **L3** was obtained as an air-sensitive, pale yellow solid after elution with Et_2O (50 mL) and solvent removal under vacuum. Yield: 183 mg, 51%. Anal. calcd. for $C_{34}H_{29}Cl_2O_6P$: C, 64.26; H, 4.60. Found: C, 64.10; H, 4.70. ^{1}H NMR ($CDCl_3$): δ/ppm = 8.12–8.05 (m, 1H, C18-H), 7.47–7.41 (m, 2H, C19-H + C20-H), 7.38–7.30 (m, 6H, C25-H + C26-H), 7.30–7.22 (m, 4H, C24-H), 7.02 (d, $^3J_{HH}$ = 8.5 Hz, 1H, C11-H), 7.00–6.93 (m, 1H, C21-H), 6.81 (d, $^3J_{HH}$ = 8.5 Hz, 1H, C10-H), 5.94 (s, 1H, C4-H), 5.60 (s, 1H, C4-H'), 4.72 (s, 2H, C12-H), 4.47–4.44 (m, 2H, C15-H), 4.43–4.40 (m, 2H, C14-H), 2.49 (q, $^3J_{HH}$ = 7.4 Hz, 2H, C2-H), 1.16 (t, $^3J_{HH}$ = 7.4 Hz, 3H, C1-H). $^{13}C\{^1H\}$ NMR ($CDCl_3$): δ/ppm = 195.9 (C5), 167.7 (C13), 166.6 (C16), 155.5 (C9), 150.3 (C3), 140.7 (d, $^1J_{CP}$ = 27.1 Hz, C22-H), 137.8 (d, $^1J_{CP}$ = 10.9 Hz, C23-H), 134.7 (C21), 134.0 (d, $^2J_{CP}$ = 20.5 Hz, C24-H), 133.7 (C8), 132.5 (C20), 131.5 (C7), 130.9 (C18), 128.8 (C26), 128.7 (C4), 128.6 (d, $^3J_{CP}$ = 6.7 Hz, C25), 128.5 (C19),

127.0 (C11), 123.3 (C6), 111.1 (C10), 66.1 (C12), 63.3 (C14), 62.4 (C15), 23.5 (C2), 12.5 (C1). $^{31}P\{^{1}H\}$ NMR ($CDCl_3$): δ/ppm = – 4.5.

Synthesis of [(η^6-*p*-cymene)$RuCl_2$(κ*P*-PPh_2(4-$C_6H_4CO_2H$))], 1.

Chart 5. Structure of **1** (numbering refers to carbon atoms).

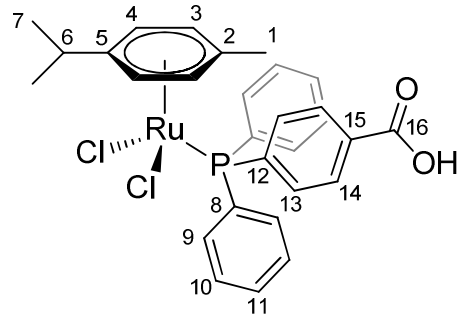

[(η^6-*p*-cymene)$RuCl_2$]$_2$ (356 mg, 0.58 mmol) and 4-(diphenylphosphino)benzoic acid (428 mg, 1.40 mmol) were dissolved in CH_2Cl_2 (15 mL). The resulting dark red solution was heated at reflux and the progress of reaction was monitored by TLC. After 4 hours, the red solution was cooled to room temperature and volatiles were removed under vacuum. The residue was dissolved in a small volume of CH_2Cl_2 and loaded on top of a silica column. Impurities were eluted with Et_2O; then a red band was collected with Me_2CO/EtOH (1:1 *v*/*v*). Complex **1** was finally obtained an air-stable red-brown powder after solvent removal under vacuum (40 °C). Yield: 485 mg, 68%. Compound **1** is soluble in DMSO, acetone and chlorinated solvents, slightly soluble in Et_2O and insoluble in H_2O. Crystals suitable for X-ray analysis were obtained by slow diffusion of hexane into a CH_2Cl_2 solution of **1** at 4°C. Anal. calcd. for $C_{29}H_{29}Cl_2O_2PRu$: C, 56.87; H, 4.77. Found: C, 56.59; H, 4.76. Mp: 160-170°C (red liquid), decomp. at 215-220°C (black liquid). IR (solid state): $\tilde{\upsilon}/cm^{-1}$ = 3600-3200w-br, 3055m, 2962m, 2872m, 1715s, 1692s ($\nu_{C16=O}$), 1599m, 1561w, 1483w, 1470w, 1435s, 1395m, 1373m-sh, 1318w, 1276m-br, 1217m, 1184m, 1116w, 1090s, 1058w, 1030w, 1018w, 999w, 909m, 857m, 799w, 767m,

747m, 728m, 695s, 675s-sh. IR (CH_2Cl_2): $\tilde{\upsilon}/cm^{-1}$ = 1733m and 1697s ($\nu_{C16=O}$), 1600m, 1560w. UV-Vis (CH_2Cl_2): λ_{max}/nm ($\varepsilon/M^{-1}\cdot cm^{-1}$) = 250 ($2.7\cdot10^4$), 375 ($1.8\cdot10^3$), 475sh ($5.2\cdot10^2$). Λ_m (CH_2Cl_2) = 0.31 $S\cdot cm^2\cdot mol^{-1}$. ^{1}H NMR ($CDCl_3$): δ/ppm = 8.03–7.99 (m, 2H, C14-H), 7.97–7.91 (m, 2H, C13-H), 7.86–7.80 (m, 4H, C9-H), 7.49–7.37 (m, 6H, C10-H + C11-H), 6.30 (br, 1H, OH), 5.24 (d, $^2J_{HH}$ = 5.6 Hz, 2H, C4-H), 5.00 (d, $^2J_{HH}$ = 5.2 Hz, 2H, C3-H), 2.87 (hept, $^3J_{HH}$ = 6.7 Hz, 1H, C6-H), 1.87 (s, 3H, C1-H), 1.12 (d, $^3J_{HH}$ = 6.9 Hz, 6H, C7-H). $^{13}C\{^1H\}$ NMR ($CDCl_3$): δ/ppm = 170.4 (C16), 140.0 (d, $^1J_{CP}$ = 43.7 Hz, C12), 134.3 (d, $^2J_{CP}$ = 11.5 Hz, C13), 134.2 (d, $^2J_{CP}$ = 10.0 Hz, C9), 133.1 (d, $^1J_{CP}$ = 45.1 Hz, C8), 130.6–130.5 (m, C11 + C15), 129.0 (d, $^3J_{CP}$ = 9.9 Hz, C14), 128.2 (d, $^3J_{CP}$ = 9.9 Hz, C10-H), 111.3 (C5), 96.3 (C2), 88.9 (d, $^2J_{CP}$ = 2.1 Hz, C3), 87.3 (d, $^2J_{CP}$ = 5.3 Hz, C4), 30.2 (C6), 21.8 (C7), 17.7 (C1). $^{31}P\{^1H\}$ NMR ($CDCl_3$): δ/ppm = 25.3.

Synthesis of [(η^6-*p*-cymene)RuCl(κ^2*P,O*-$PPh_2(2\text{-}C_6H_4CO_2)$)], 2.

Chart 6. Structure of **2** (numbering refers to carbon atoms).

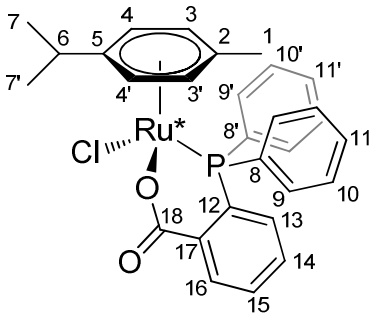

[(η^6-*p*-cymene)$RuCl_2$]$_2$ (190 mg, 0.311 mmol) and 2-(diphenylphosphino)benzoic acid (232 mg, 0.757 mmol) were dissolved in CH_2Cl_2 (20 mL). The resulting brick red solution was heated at reflux and the progress of reaction was monitored by TLC and ^{31}P NMR spectroscopy. Evolution of HCl was detected with a pH paper placed on top of the reflux condenser. After 4 hours, the orange-red solution was cooled to room temperature and volatiles were removed under vacuum. The orange residue was suspended in Et_2O and filtered. The solid was dissolved in CH_2Cl_2 then ^{i}PrOH (1-2 mL) and Et_2O were

added with intense stirring. Compound **2** readily precipitated as an air-stable orange-brown powder. The solid was filtered, washed with Et_2O (3x5 mL) and dried under vacuum (40°C). Yield: 269 mg, 75%. The precipitation procedure was repeated on the filtrate solution (90% yield).

Alternative procedure: K[PPh_2(2-$C_6H_4CO_2$)] (74 mg, 0.213 mmol) was added to a suspension of [(η^6-*p*-cymene)$RuCl_2$]$_2$ (56 mg, 0.091 mmol) in ^{i}PrOH (5 mL). The reaction mixture was stirred at room temperature for 30 hours and the progress of reaction was monitored by TLC. Therefore, the orange suspension was filtered, the colourless precipitate washed with CH_2Cl_2 and volatiles were removed under vacuum from the filtrate solution. The residue was dissolved into a small volume of CH_2Cl_2 and loaded on top of a silica column. An orange band was eluted with CH_2Cl_2:THF (progressively decreasing *v/v* ratio). Complex **2** was finally obtained as an orange-brown powder after solvent removal under vacuo (40°C). Yield: 59 mg, 57%.

Compound **2** is soluble in MeOH and DMSO, moderately soluble in chlorinated solvents and insoluble in H_2O. Crystals suitable for X-ray analysis were obtained from $CHCl_3$ solutions of **2** layered with hexane or Et_2O and settled aside at -20°C. Anal. calcd. for $C_{29}H_{28}ClO_2PRu$: C, 60.47; H, 4.90. Found: C, 60.12; H, 5.07. Mp: decomp. at 130°C (dark brown solid). IR (solid state): $\tilde{\upsilon}$/cm^{-1} = 3053w, 2962w, 2926w, 2869w, 1619s-sh, 1604s ($\nu_{CO2,as}$), 1583m, 1557m, 1482m, 1469m, 1434m, 1386m, 1328s ($\nu_{CO2,s}$), 1284m, 1253m, 1186w, 1160w, 1143w, 1118m, 1096m, 1060m, 1030w, 998w, 888w, 846m, 800w, 747m, 728m, 694s. UV-Vis (CH_2Cl_2): λ_{max}/nm (ε/M$^{-1}\cdot$cm^{-1}) = 350 ($1.5\cdot10^3$). Λ_m (CH_2Cl_2) = 0.92 S$\cdot$cm$^2\cdot$mol^{-1}. ^{1}H NMR ($CDCl_3$): δ/ppm = 8.23 (dd, *J* = 7.1, 4.5 Hz, 1H, C16-H), 7.97 (dd, *J* = 11.0, 7.8 Hz, 2H, C9-H), 7.68–7.63 (m, 1H, C11-H), 7.59–7.51 (m, 5H, C10-H + C10'-H + C11'-H), 7.51–7.42 (m, 3H, C9'-H + C15-H), 7.33 (t, *J* = 7.5 Hz, 1H, C14-H), 6.83 (dd, *J* = 11.1, 7.8 Hz, 1H, C13-H), 6.08 (s-br, 1H, C4-H), 5.75 (s-br, 1H, C3-H), 5.53 (s-br, 1H, C3'-H), 5.19 (s-br, 1H, C4'-H), 2.78–2.65 (m, 1H, C6-H), 1.97 (s, 3H, C1-H), 1.06, 0.60 (d, $^3J_{HH}$ = 6.8 Hz, 3H, C7-H + C7'-H). ^{13}C{^{1}H} NMR ($CDCl_3$): δ/ppm = 172.3 (C18), 138.6–138.1 (m, C17), 135.3 (d, $^2J_{CP}$ = 10.6 Hz, C9),

133.2 (d, $^{1}J_{CP}$ = 49.3 Hz, C8'), 132.3 (d, $^{3}J_{CP}$ = 2.5 Hz, C16) 132.2 (d, $^{2}J_{CP}$ = 10.5 Hz, C9'), 132.1 (C11), 131.7 (C13), 131.1 (d, J_{CP} = 1.5 Hz, C14 or C15), 131.0 (d, J_{CP} = 1.7 Hz, C14 or C15), 129.6 (d, $^{1}J_{CP}$ = 44.7 Hz, C8), 129.3 (d, $^{3}J_{CP}$ = 9.7 Hz, C10 or C10'), 129.1 (d, $^{3}J_{CP}$ = 10.3 Hz, C10 or C10'), 128.1 (d, $^{1}J_{CP}$ = 49.6 Hz, C12), 108.9 (C5), 97.1 (br, C3), 92.0 (C2), 90.9 (C4), 85.0 (C3'), 84.3 (C4'), 29.7 (C6), 23.0, 19.1 (C7 + C7'), 17.7 (C1). $^{31}P\{^{1}H\}$ NMR ($CDCl_3$): δ/ppm = 30.5.

Synthesis of [(η^6-*p*-cymene)$RuCl_2$(κ*P*-PPh_2(2-C_6H_4OCO-EA))], 3.

Chart 7. Structure of **3** (numbering refers to carbon atoms).

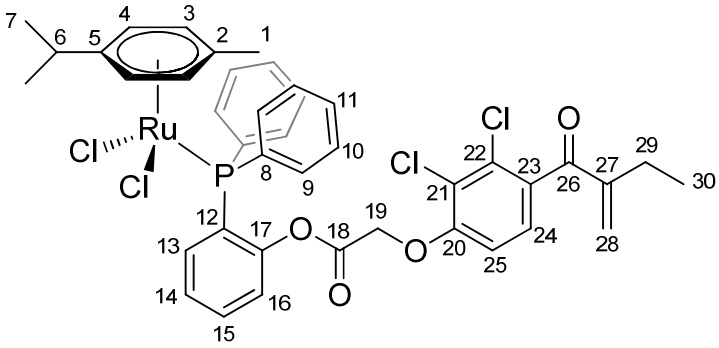

[(η^6-*p*-cymene)$RuCl_2$]$_2$ (156 mg, 0.254 mmol) and **L1** (358 mg, 0.636 mmol) were dissolved in $CHCl_3$ (25 mL) and the resulting brick red solution was heated at reflux for 20 hours. The final dark brown solution was cooled to room temperature and then volatiles were removed under vacuum. The dark residue was suspended in Et_2O and filtered. The solid was then dissolved in CH_2Cl_2 (4 mL), and Et_2O/hexane 2:1 *v*/*v* (30 mL) was added with intense stirring. Compound **3** precipitated as an air-stable brown-red powder from a dark green solution. The solid was filtered, washed with hexane (3x5 mL) and dried under vacuum (room temperature). Yield: 285 mg, 65%. Compound **3** is soluble in DMSO and chlorinated solvents, less soluble in acetone and MeOH and insoluble in H_2O. Anal. calcd. for $C_{41}H_{39}Cl_4O_4PRu$: C, 56.63; H, 4.52. Found: C, 56.50; H, 4.69. Mp: decomp. at 184-188°C (black liquid). IR (solid state): $\tilde{\upsilon}/cm^{-1}$ = 3053w, 2970w, 2934w, 2875w, 1782s ($\nu_{C18=O}$), 1663m ($\nu_{C26=O}$),

1625w, 1582m ($\nu_{C27=C28}$), 1466m, 1436s, 1379m, 1340w, 1303m, 1264m, 1201s, 1151s, 1115m, 1074s, 1031m, 1000m, 937w, 896w, 853w, 817m, 801m, 780m, 749m, 696s. IR (CH_2Cl_2): $\tilde{\upsilon}/cm^{-1}$ = 1782s ($\nu_{C18=O}$), 1667s ($\nu_{C26=O}$), 1587s ($\nu_{C27=C28}$). UV-Vis (CH_2Cl_2): λ_{max}/nm ($\varepsilon/M^{-1}\cdot cm^{-1}$) = 250 ($3.2\cdot10^4$), 370 ($1.9\cdot10^3$), 470sh ($6.2\cdot10^2$). Λ_m (CH_2Cl_2) = 0.27 $S\cdot cm^2\cdot mol^{-1}$. ^1H NMR ($CDCl_3$): δ/ppm = 7.75–7.67 (m, 4H, C9-H), 7.65–7.57 (m, 1H, C14-H), 7.53–7.42 (m, 1H, C15-H), 7.39–7.23 (m, 8H, C10-H, C11-H, C13-H + C15-H), 6.94 (d, $^3J_{HH}$ = 8.3 Hz, 1H, C24-H), 6.44 (d, $^3J_{HH}$ = 8.3 Hz, 1H, C25-H), 5.92 (s, 1H, C28-H), 5.55 (s, 1H, C28-H'), 5.31 (s, 2H, C4-H), 4.95 (s, 2H, C3-H), 4.54 (s, 2H, C19-H), 2.94 (hept, $^3J_{HH}$ = 6.3 Hz, 1H, C6-H), 2.45 (q, $^3J_{HH}$ = 7.2 Hz, 2H, C29-H), 1.88 (s, 3H, C1-H), 1.24 (d, $^3J_{HH}$ = 6.7 Hz, 6H, C7-H), 1.13 (t, $^3J_{HH}$ = 7.4 Hz, 3H, C30-H). $^{13}C\{^1H\}$ NMR ($CDCl_3$): δ/ppm = 195.9 (C26), 165.9 (C18), 155.2 (C20), 151.5 (C17), 150.3 (C27), 135.5 (d, $^2J_{CP}$ = 6.9 Hz, C13), 134.6 (d, $^2J_{CP}$ = 9.7 Hz, C9), 133.5 (C21), 132.5 (C15), 131.1 (C22), 130.7 (d, $^1J_{CP}$ = 43.4 Hz, C8), 130.5 (C11), 128.6 (C28), 128.0 (d, $^3J_{CP}$ = 10.3 Hz, C10), 127.2 (d, $^1J_{CP}$ = 39.8 Hz, C12), 127.1 (C24), 125.9 (d, $^3J_{CP}$ = 8.3 Hz, C14), 123.5 (d, $^3J_{CP}$ = 3.4 Hz, C16), 122.9 (C23), 112.4 (d, $^2J_{CP}$ = 3.6 Hz, C5), 111.5 (C25), 97.8 (C2), 87.9 (d, $^2J_{CP}$ = 3.4 Hz, C4), 87.7 (C3), 66.6 (C19), 30.5 (C6), 23.5 (C29), 22.1 (C7), 18.2 (C1), 12.5 (C30). $^{31}P\{^1H\}$ NMR ($CDCl_3$): δ/ppm = 25.0.

Synthesis of [(η^6-*p*-cymene)$RuCl_2$(κ*P*-PPh_2(4-$C_6H_4CO_2CH_2CH_2OCO$-EA))], 4.

Chart 8. Structure of **4** (numbering refers to carbon atoms).

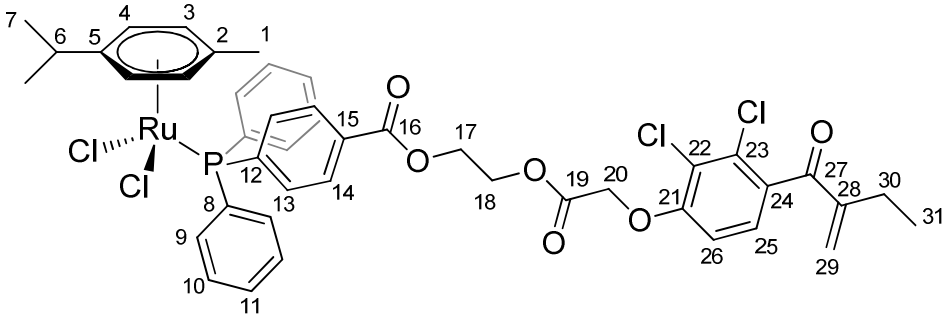

The compound was prepared according to a modified literature procedure.[10a] $[(\eta^6\text{-}p\text{-cymene})RuCl_2]_2$ (141 mg, 0.229 mmol) and **L2** (367 mg, 0.577 mmol) were dissolved in $CHCl_3$ (20 mL) and the resulting brick-red solution was heated at reflux for 18 hours. The final dark red solution was cooled to room temperature and volatiles were removed under vacuum. The red-brown residue was suspended in Et_2O and filtered. The solid was then dissolved in a small volume of CH_2Cl_2 and the solution diluted with ^{i}PrOH. Addition of hexane with intense stirring caused the precipitation of **4** an air-stable red-brown powder. The solid was filtered, washed with Et_2O (3x5 mL) and dried under vacuum (40°C). Yield: 291 mg, 67%. Anal. calcd. for $C_{44}H_{43}Cl_4O_6PRu$: C, 56.12; H, 4.60. Found: C, 56.30; H, 4.52. IR (solid state): $\tilde{\upsilon}/cm^{-1}$ = 3036w, 2964m, 2925w, 2872w, 2849w, 1761m ($\nu_{C19=O}$), 1721m ($\nu_{C16=O}$), 1665m ($\nu_{C27=O}$), 1599w-sh, 1585m ($\nu_{C28=C29}$), 1562w, 1483w, 1469m, 1436m, 1396m, 1385m, 1339w, 1285m-sh, 1262s, 1197s, 1187s, 1120m, 1108m, 1081s, 1030m, 1018s, 1002m, 943w, 896w, 846w, 801m, 747s, 722m, 697s, 665m. IR (CH_2Cl_2): $\tilde{\upsilon}/cm^{-1}$ = 1765m ($\nu_{C16=O}$), 1725s ($\nu_{C19=O}$), 1667m ($\nu_{C27=O}$), 1599w, 1587m ($\nu_{C28=C29}$). UV-Vis (CH_2Cl_2): λ_{max}/nm ($\varepsilon/M^{-1}\cdot cm^{-1}$) = 245 ($4.0\cdot10^4$), 374 ($2.0\cdot10^3$), 465sh ($7.4\cdot10^2$). Λ_m (CH_2Cl_2) = 0.91 $S\cdot cm^2\cdot mol^{-1}$. ^{1}H NMR ($CDCl_3$): δ/ppm = 7.94–7.89 (m, 4H, C13-H + C14-H), 7.86–7.78 (m, 4H, C9-H), 7.47–7.38 (m, 6H, C10-H + C11-H), 7.11 (d, $^3J_{HH}$ = 8.3 Hz, 1H, C25-H), 6.82 (d, $^3J_{HH}$ = 8.4 Hz, 1H, C26-H), 5.92 (s, 1H, C29-H), 5.58 (s, 1H, C29-H'), 5.23 (d, $^3J_{HH}$ = 5.6 Hz, 2H, C3-H or C4-H), 4.99 (d, $^3J_{HH}$ = 5.4 Hz, 2H, C4-H or C3-H), 4.77 (s, 2H, C20-H), 4.51 (s, 4H, C17-H + C18-H), 2.86 (hept, $^3J_{HH}$ = 6.7 Hz, 1H, C6-H), 2.45 (q, $^3J_{HH}$ = 7.4 Hz, 2H, C30-H), 1.86 (s, 3H, C1-H), 1.16–1.09 (m, 9H, C7-H + C31-H). $^{13}C\{^1H\}$ NMR ($CDCl_3$): δ/ppm = 195.7 (C27), 167.5 (C19), 165.7 (C16), 155.3 (C21), 150.1 (C28), 139.5 (d, $^1J_{CP}$ = 44.3 Hz, C12), 134.5 (d, $^2J_{CP}$ = 9.2 Hz, C13), 134.3 (d, $^2J_{CP}$ = 9.6 Hz, C9), 133.8 (C22), 133.3 (d, $^1J_{CP}$ = 45.9 Hz, C8), 131.3 (C23), 130.7 (C11), 130.5 (C15), 128.8–128.5 (m, C14 + C29), 128.3 (d, $^3J_{CP}$ = 9.8 Hz, C10), 126.9 (C25), 123.3 (C24), 111.4 (d, $^2J_{CP}$ = 2.4 Hz, C5), 111.0 (C26), 96.4 (C2), 89.0 (d, $^2J_{CP}$ = 2.0 Hz, C3 or

C4), 87.4 (d, $^{2}J_{CP}$ = 5.4 Hz, C4 or C3), 66.1 (C20), 63.3, 62.4 (C17 + C18), 30.3 (C6), 23.4 (C30), 21.9 (C7), 17.8 (C1), 12.4 (C31). $^{31}P\{^{1}H\}$ NMR ($CDCl_3$): δ/ppm = 25.3.

Formation of [(η^6-arene)$RuCl_2$(κ*P*-PPh_2(2-$C_6H_4CO_2CH_2CH_2OCO$-EA))] (arene = *p*-cymene, 5a; arene = C_6H_6, 5b).

Chart 9. Structure of **5a**,**b** (numbering refers to carbon atoms).

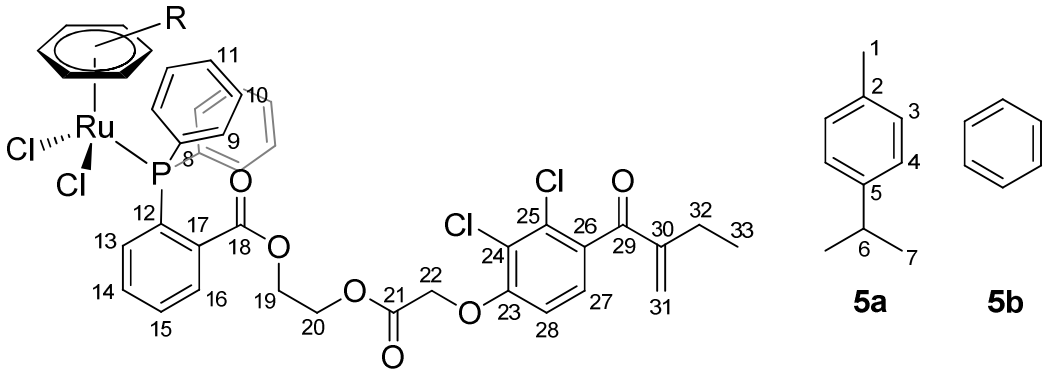

A brick red solution of [(η^6-*p*-cymene)$RuCl_2$]$_2$ (67 mg, 0.11 mmol) and **L3** (150 mg, 0.236 mmol) in $CDCl_3$ (5 mL) was stirred at room temperature and periodically sampled for NMR analysis (^{1}H, ^{31}P). After 4.5 hours, the conversion of the starting materials was complete, with formation of **5a** (≈ 85% NMR yield) and other products. Hence the solution progressively darkened with release of *p*-cymene (4.5 h: 10%, 18h: 38%, 26h: 82%, 5d: 88%) and formation of another P-containing species (^{31}P: δ = 63 ppm). A red-brown solid was isolated from the reaction mixture. This material rapidly converted into a paramagnetic green solid upon air exposure. The reaction was repeated with [(η^6-C_6H_6)$RuCl_2$]$_2$ with a similar outcome: initial formation of **5b** was soon followed by release of benzene (5.5h: 24%, 10.5h: 50%, 24h: quantitative) and formation of other P-containing species (^{31}P: δ = 72.9, 63.1, 31.4 ppm).

5a. ^{1}H NMR ($CDCl_3$): δ/ppm = 8.29–8.22 (m, 1H, C16-H), 7.84–7.75 (m, 4H, C9-H), 7.64–7.53 (m, 2H, C14-H + C15-H), 7.30–7.19 (m, 6H, C10-H + C11-H), 7.09 (d, $^{3}J_{HH}$ = 8.7 Hz, 1H, C27-H), 7.02–6.93 (m, 1H, C13-H), 6.78 (d, $^{3}J_{HH}$ = 8.6 Hz, 1H, C28-H), 5.93 (s, 1H, C31-H), 5.57 (s, 1H, C31-H'),

5.43 (d, $^{3}J_{HH}$ = 6.1 Hz, 2H, C3-H/C4-H), 5.35 (d, $^{3}J_{HH}$ = 5.8 Hz, 2H, C3-H/C4-H), 4.77 (s, 2H, C22-H), 4.29–4.24 (m, 2H, C19-H/C20-H), 3.79–3.74 (m, 2H, C19-H/C20-H), 2.74 (hept, $^{3}J_{HH}$ = 6.9 Hz, 1H, C6-H), 2.46 (q, $^{3}J_{HH}$ = 7.4 Hz, 2H, C32-H), 1.87 (s, 3H, C1-H), 1.20 (t, $^{3}J_{HH}$ = 7.1 Hz, 3H, C33-H), 1.13 (d, $^{3}J_{HH}$ = 7.0 Hz, 6H, C7-H). $^{31}P\{^{1}H\}$ NMR ($CDCl_3$): δ/ppm = 26.0.

5b. ^{1}H NMR ($CDCl_3$): δ/ppm = 8.28–8.21 (m, 1H, C16-H), 7.75–7.68 (m, 4H, C9-H), 7.50–7.42 (m, 1H, C14-H/C15-H), 7.37–7.25 (m, 8H, C10-H + C11-H + C13-H + C14-H/C15-H), 7.11 (d, $^{3}J_{HH}$ = 8.5 Hz, 1H, C27-H), 6.80 (d, $^{3}J_{HH}$ = 8.5 Hz, 1H, C28-H), 5.78 (s, 1H, C31-H), 5.60 (s, 6H, Ru-C_6H_6), 5.59 (s, 1H, C31-H'), 4.79 (s, 2H, C22-H), 4.26–4.21 (m, 2H, C19-H/C20-H), 3.81–3.76 (m, 2H, C19-H/C20-H), 2.49 (q, $^{3}J_{HH}$ = 7.1 Hz, 2H, C32-H), 1.23 (t, $^{3}J_{HH}$ = 7.0 Hz, 3H, C33-H). $^{31}P\{^{1}H\}$ NMR ($CDCl_3$): δ/ppm = 28.9.

Synthesis of K[PPh_2(2-$C_6H_4CO_2$)].

Chart 10. Structure of K[PPh_2(2-$C_6H_4CO_2$)].

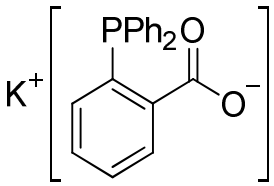

An ethanolic solution of KOH (2.1 mL, 0.135 M) was added to a solution of 2-(diphenylphosphino)benzoic acid (88 mg, 0.287 mmol) in EtOH (4 mL). Precipitation of a colourless solid was observed in a few minutes. The suspension was stirred at room temperature for 30 minutes, then filtered. The resulting colourless solid was washed with few mL of EtOH, Et_2O then dried under vacuum (40°C). Yield: 79 mg, 84%. K[PPh_2(2-$C_6H_4CO_2$)] is soluble in MeOH and DMSO, less soluble in H_2O and and insoluble in chlorinated solvents. Anal. calcd. for $C_{19}H_{14}KO_2P$: C, 66.26; H, 4.10. Found: C, 65.89; H, 4.06. IR (solid state): $\tilde{\upsilon}/cm^{-1}$ = 3656w, 3064w, 3042w, 1593s ($\nu_{CO2,as}$), 1574s, 1552s, 1476m, 1452w, 1434m, 1375s ($\nu_{CO2,s}$), 1328w, 1307w, 1279w, 1205w, 1179w, 1156w, 1108w, 1097w, 1087w, 1070w, 1027w, 998w, 836m, 823w-sh, 747s, 698s, 684m-sh, 654w. ^{1}H NMR

(CD_3OD): δ/ppm = 7.83–7.73 (m, 1H), 7.39–7.13 (m, 12H), 6.89–6.76 (m, 1H). $^{31}P\{^1H\}$ NMR (CD_3OD): δ/ppm = –8.2. ^1H NMR (D_2O): δ/ppm = 7.64–7.57 (m, 1H), 7.49–7.29 (m, 10H), 7.04–6.97 (m, 1H). $^{31}P\{^1H\}$ NMR (D_2O): δ/ppm = –9.6.

2) Electrochemistry and Spectroelectrochemistry.

Electrochemical measurements were performed with a Princeton Applied Research (PAR) 273A potenziostat/galvanostat, interfaced to a computer employing PAR M270 electrochemical software. All measurements were carried out at room temperature using 0.2 M [^{n}Bu$_4$N][PF_6] in CH_2Cl_2 as supporting electrolyte. HPLC grade dichloromethane (Sigma Aldrich) was stored under argon over 3Å molecular sieves. [^{n}Bu$_4$N][PF_6] (Fluka, electrochemical grade) and Cp_2Fe (Fluka) were used without further purification. Cyclic voltammetry was carried out in a three-electrode home-built cell. The working and the counter electrode consisted of a platinum disk electrode and a platinum wire spiral, respectively, both sealed in a glass tube. A quasi-reference platinum electrode was employed as a reference. The cell was pre-dried by heating under vacuum and filled with argon. The Schlenk-type construction of the cell maintained anhydrous and anaerobic conditions. The solution of supporting electrolyte, prepared under argon, was introduced into the cell and the working electrode was cycled several times between the anodic and cathodic limits of interest until there was no change in the charging current. The analyte was then introduced ([Ru] = 0.7-4.5·10^{-3} mol·L^{-1}) and voltammograms were recorded; then a small amount of ferrocene was added and the voltammograms repeated. Potentials were determined by placing $E_{1/2}$ = +0.39 V *vs.* SCE for the Cp_2Fe^+/Cp_2Fe couple.[38] The ohmic drop was not compensated.

Controlled potential coulometry (CPC) and linear sweep voltammetry (LSW) were performed in a H-shaped cell with anodic and cathodic compartments separated by a sintered-glass disk. For CPC, the working macroelectrode was a platinum gauze; a platinum spiral was used as the counter electrode. For LSW, the working electrode was rotating-disk electrode and the platinum gauze was used as the

counter-electrode. The experiment was performed as follows. Compound **1** ($1.7 \cdot 10^{-2}$ mmol) was dissolved in 10 mL of the electrolyte solution. A series of electrolysis/voltammetry experiments were performed until the compounds was fully oxidized to $\mathbf{1}^+$. Electrolysis was performed at a constant potential E = E°' + 0.1 V while LSW was performed between E°'± 0.7 V with a scan rate of 20 mV/s.
In LSW experiments, the ratio between the oxidation and reduction currents is directly proportional to the $\mathbf{1}/\mathbf{1}^+$ ratio in solution. The total electric charge determined by CPC was in agreement with the $\mathbf{1}/\mathbf{1}^+$ ratio in solution, as determined by LSW, for a monoelectronic process. UV-Vis and IR spectroelectrochemical measurements were carried out using an optically transparent thin-layer electrochemical (OTTLE) cell equipped with CaF_2 windows, platinum minigrid working and auxiliary electrodes and silver wire pseudo-reference electrode.[39] The in situ spectroelectrochemical experiments were performed by collecting IR/UV-Vis spectra of compounds **1**,**3** and **4** during the oxidation process obtained by linearly increasing the initial working potential with a scan rate of 0.5 mV/min. In order to check the stability of the electro-generated cationic species, the potential scan was reversed and the spectra were re-acquired.

3) X-ray crystallography.

Crystal data and collection details for **1** and **2** are reported in Table 5. Data were recorded on a Bruker APEX II diffractometer equipped with a CCD detector using Mo–Kα radiation. Data were corrected for Lorentz polarization and absorption effects (empirical absorption correction SADABS).[40] The structures were solved by direct methods and refined by full-matrix least-squares based on all data using F^2.[41] Hydrogen atoms were fixed at calculated positions and refined by a riding model. All non-hydrogen atoms were refined with anisotropic displacement parameters.

Table 5. Crystal data and measurement details for **1** and **2**.

	1	**2**
Formula	$C_{29}H_{31}Cl_2O_3PRu$	$C_{29}H_{28}ClO_2PRu$
FW	630.48	576.00
T, K	100(2)	100(2)
λ, Å	0.71073	0.71073
Crystal system	Monoclinic	Monoclinic
Space group	$P2_1/n$	$P2_1/c$
a, Å	9.7510(3)	15.373(2)
b, Å	16.2442(5)	13.900(2)
c, Å	17.3619(5)	23.827(4)
β,°	100.538(2)	94.239(4)
Cell Volume, Å^3	2703.69(14)	5077.5(14)
Z	4	8
D_c, g·cm^{-3}	1.549	1.507
μ, mm^{-1}	0.866	0.810
F(000)	1288	2352
Crystal size, mm	0.15 x 0.13 x 0.11	0.18 x 0.16 x 0.12
θ limits,°	1.731-26.538	1.328 - 25.100
Reflections collected	43361	42443
Independent reflections	5620 [R_{int} = 0.0580]	9036 [R_{int} = 0.1154]
Data / restraints /parameters	5620 / 3 / 334	9036 / 36 / 619
Goodness on fit on F^2	1.074	1.132
R_1 ($I > 2\sigma(I)$)	0.0330	0.0728
wR_2 (all data)	0.0875	0.1496
Largest diff. peak and hole, e Å^{-3}	0.717 / –0.579	1.023 / –1.472

4. In vitro cytotoxicity investigation.

Cell lines.

In vitro cytotoxicity investigations were carried out by using the mouse embryo fibroblasts balb/3T3 clone A31 cell line (CCL-163) and the BxPC3 human pancreas adenocarcinoma cell line (CRL-1687). Both cell lines were purchased from the American Type Culture Collection (ATCC).

Mouse embryo fibroblasts Balb/3T3 Clone A31 were maintained in Dulbecco's Modified Eagle Medium (DMEM) (Sigma-Aldrich, Italy) supplemented with 4 mM of L-glutamine (Lonza, New Hampshire), 1% of penicillin (streptomycin solution, 10,000 U/mL = 10 mg/mL; Lonza, New Hampshire), 10% of calf serum (Sigma-Aldrich, Italy) and antimycotic (complete DMEM). Prior to incubation with the compounds of interest, Balb/3T3 Clone A31 cells were seeded in 96 wells tissue culture polystyrene plates at a density of $2x10^3$ per well in a volume of 100 μL of medium and allowed to proliferate for 24 hours at 37°C in a 5% CO_2 modified atmosphere.

BxPC-3 cells were maintained in RPMI-1640 medium (Sigma-Aldrich, Italy) containing 4 mM of L-glutamine (Lonza, New Hampshire), 1% of sodium pyruvate (Sigma-Aldrich, Italy), 1% of penicillin/streptomycin solution (10,000 U/mL = 10 mg/mL; Lonza, New Hampshire), 10% of fetal serum (Sigma-Aldrich, Italy) and antimycotic (complete RPMI-1640). Prior to incubation with the compound of interest, BxPC-3 cells were seeded in 96 wells tissue culture polystyrene plates at a density of $1x10^4$ per well in a volume of 100 μL of medium and allowed to proliferate for 24 hours at 37°C in a 5% CO_2 modified atmosphere.

Cytotoxicity assay.

Stock solutions (40 mM) in DMSO were prepared for each compound to be tested. Solutions at different concentration, comprised in the range of 1-80 μM, were obtained by serial dilution of stock solution in cell culture media. Cells incubated with culture media containing appropriate concentration of DMSO were used as control. Cells were incubated with the different concentration of compounds for 72 hours at 37°C in a 5% CO_2 modified atmosphere. At the end of the incubation time, cell viability was assessed by mean of WST-1 tetrazolium salt reagent (Roche). Briefly, cells were incubated for 4

hours with WST-1 reagent diluted 1:10, at 37°C and 5% CO_2. Measurements of formazan dye absorbance, which directly correlates with the number of viable cells, were carried out with a micro-plate reader (Biorad, Milan) at 450 nm, using 655 nm as reference wavelength. The 50% inhibitory concentration of the tested compound (IC_{50}) refers to the concentration at which 50% of cell death in respect to the control is observed. All the in vitro biological tests were performed on triplicate for each concentration, and the data are reported as mean ± standard deviation.

5. Interaction with model proteins

Metal complexes/protein adducts were prepared by adding the appropriate Ru complex dissolved in DMSO to a solution of the protein (10^{-3} M) in 20 mM ammonium acetate solution buffered at pH = 6.8 (final metal complex/protein ratio = 3:1; final adduct concentration = 10^{-4} M). The solutions were incubated for 72 h at 37 °C. After a 20-fold dilution with water, ESI–MS spectra were recorded by direct introduction of the sample at a flow rate of 5 μL/min in an LTQ Orbitrap high-resolution mass spectrometer (Thermo, San Jose, CA, USA), equipped with a conventional ESI source. The working conditions were as follows: spray voltage 3.1 kV, capillary voltage 45 V, capillary temperature 220 °C. The sheath and the auxiliary gases were set, respectively, at 17 (arbitrary units) and 1 (arbitrary units). Xcalibur 2.0 software (Thermo) was used for acquisition, and monoisotopic and average deconvoluted masses were obtained by using the integrated Xtract tool. For spectrum acquisition a nominal resolution (at m/z 400) of 100,000 was used.

Acknowledgements

We gratefully thank the University of Pisa for financial support (PRA 2015: "*Sintesi e studio delle proprietà di composti di metalli di transizione come agenti antitumorali"*).

Supporting Information Available

Synthetic details, electrochemistry, X-ray structure of **1**, ESI-MS spectra. CCDC reference numbers 1534352 (**1**) and 1534353 (**2**) contain the supplementary crystallographic data for the X-ray studies reported in this paper. These data can be obtained free of charge at www.ccdc.cam.ac.uk/conts/retrieving.html (or from the Cambridge Crystallographic Data Centre, 12, Union Road, Cambridge CB2 1EZ, UK; fax: (internat.) +44-1223/336-033; e-mail: deposit@ccdc.cam.ac.uk).

References

1 a) E. Alessio, Eur. J. Inorg. Chem. 2017, 1549-1560. b) A. Bijelic, S. Theiner, B. K. Keppler, A. Rompel, J. Med. Chem. 2016, 59, 5894-5903. c) R. Trondl, P. Heffeter, C. R. Kowol, M. A. Jakupec, W. Berger, B. K. Keppler, Chem. Sci. 2014, 5, 2925-2932.

2 I. Bratsos, T. Gianferrara, E. Alessio, C. G. Hartinger, M. A. Jakupec, B. K. Keppler, in Bioinorganic Medicinal Chemistry, ed. E. Alessio, Wiley-VCH, Weinheim 2011, 151-174.

3 a) A. K. Singh, D. S. Pandey, Q. Xu, P. Braunstein, Coord. Chem. Rev. 2014, 270–271, 31–56. b) M. V. Babak, D. Plazuk, S. M. Meier, H. J. Arabshahi, J. Reynisson, B. Rychlik, A. Błauz, K. Szulc, M. Hanif, S. Strobl, A. Roller, B. K. Keppler, C. G. Hartinger, Chem. Eur. J. 2015, 21, 5110-5117. c) A. L. Noffke, A. Habtemariam, A. M. Pizarro, P. J. Sadler, Chem. Commun. 2012, 48, 5219–5246. d) C. G. Hartinger, P. J. Dyson, Chem. Soc. Rev. 2009, 38, 391-401. e) A. Habtemariam, M. Melchart, R. Fernàndez, S. Parsons, I. D. H. Oswald, A. Parkin, F. P. A. Fabbiani, J. E. Davidson, A. Dawson, R. E. Aird, D. I. Jodrell, P. J. Sadler, J. Med. Chem. 2006, 49, 6858 - 6868.

4 a) B. S. Murray, M. V. Babak, C. G. Hartinger, P. J. Dyson, Coord. Chem. Rev. 2016, 306, 86–114. b) A. Weiss, R. H. Berndsen, M. Dubois, C. Müller, R. Schibli, A. W. Griffioen, P. J. Dyson,

P. Nowak-Sliwinska, Chem. Sci. 2014, 5, 4742–4748. c) Z. Adhireksan, G. E. Davey, P. Campomanes, M. Groessl, C. M. Clavel, H. Yu, A. A. Nazarov, C. H. F. Yeo, W. H. Ang, P. Dröge, U. Rothlisberger, P. J. Dyson, C. A. Davey, Nature Commun. 2014, 5, 3462.

5 a) E. Păunescu, S. McArthur, M. Soudani, R. Scopelliti, P. J. Dyson, Inorg. Chem. 2016, 55, 1788−1808. b) R. Sáez, J. Lorenzo, M. J. Prieto, M. Font-Bardia, T. Calvet, N. Omeñaca, M. Vilaseca, V. Moreno, J. Inorg. Biochem. 2014, 136, 1–12. c) A. Castonguay, C. Doucet, M. Juhas, D. Maysinger, J. Med. Chem. 2012, 55, 8799-8806. d) A. K. Renfrew, R. Scopelliti, P. J. Dyson, Inorg. Chem. 2010, 49, 2239–2246. e) L. Biancalana, G. Pampaloni, F. Marchetti, Chimia 2017, 71, 573–579.

6 S. Parveen, M. Hanif, S. Movassaghi, M. Sullivan, M. Kubanik, M. A. Shaheen, T. Söhnel, S. M. F. Jamieson, C. G. Hartinger, Eur. J. Inorg. Chem. 2017, 1721-1727.

7 a) M. Patra, T. C. Johnstone, K. Suntharalingam, S. J. Lippard, Angew. Chem. Int. Ed. 2016, 55, 2550–2554. b) S. Banerjee, A. R. Chakravarty, Acc. Chem. Res. 2015, 48, 2075−2083. c) Q. Cheng, H. Shi, H. Wang, Y. Min, J. Wang, Y. Liu, Chem. Commun. 2014, 50, 7427-7430. d) K. J. Kilpin, P. J. Dyson, Chem. Sci. 2013, 4, 1410–1419.

8 W. H. Ang, L. J. Parker, A. De Luca, L. Juillerat-Jeanneret, C. J. Morton, M. Lo Bello, M. W. Parker, P. J. Dyson, Angew. Chem. Int. Ed. 2009, 48, 3854-3857.

9 J. D. Collier, M. K. Bennett, A. Hall, A. R. Cattan, R. Lendrum, M. F. Bassendine, Gut. 1994, 35, 266–269.

10 a) G. Agonigi, T. Riedel, S. Zacchini, E. Păunescu, G. Pampaloni, N. Bartalucci, P. J. Dyson, F. Marchetti, Inorg. Chem. 2015, 54, 6504−6512. b) W. H. Ang, A. De Luca, C. Chapuis-Bernasconi, L. Juillerat-Jeanneret, M. Lo Bello, P. J. Dyson, ChemMedChem 2007, 2, 1799-1806. c) L. Biancalana, L. K. Batchelor, A. De Palo, S. Zacchini, G. Pampaloni, P. J. Dyson, F. Marchetti, Dalton Trans. 2017, 46, 12001–12004. d) E. Păunescu, M. Soudani, P. Martin, R. Scopelliti, M. Lo

Bello and P. J. Dyson, Organometallics 2017, 36, 3313−3321. e) E. Păunescu, M. Soudani, C. M. Clavel and P. J. Dyson, J. Inorg. Biochem. 2017, 175, 198–207.

11 L. J. Parker, L. C. Italiano, C. J. Morton, N. C. Hancock, D. B. Ascher, J. B. Aitken, H. H. Harris, P. Campomanes, U. Rothlisberger, A. De Luca, M. Lo Bello, W.-H. Ang, P. J. Dyson, M. W. Parker, Chem. Eur. J. 2011, 17, 7806-7816.

12 a) S. Chatterjee, I. Biondi, P. J. Dyson, A. Bhattacharyya, J. Biol. Inorg. Chem. 2011, 16, 715-724. b) K. Johansson, M. Ito, C. M. S. Schophuizen, S. M. Thengumtharayil, V. D. Heuser, J. Zhang, M. Shimoji, M. Vahter, W. H. Ang, P. J. Dyson, A. Shibata, S. Shuto, Y. Ito, H. Abe, R. Morgenstern, Mol. Pharmaceutics 2011, 8, 1698-1708.

13 a) N. Rao Palepu, S. Adhikari, R. Premkumar, J. Akalesh, K. Verma, S. L. Shepherd, R. M. Phillips, W. Kaminsky, M. R. Kollipara, Appl. Organometal. Chem., 2017, 31, 3640.

14 a) A. Kurzwernhart, W. Kandioller, S. Bächler, C. Bartel, S. Martic, M. Buczkowska, G. Mühlgassner, M. A. Jakupec, H.-B. Kraatz, P. J. Bednarski, V. B. Arion, D. Marko, B. K. Keppler, C. G. Hartinger, J. Med. Chem. 2012, 55, 10512-10522. b) C. Aliende, M. Pérez-Manrique, F. A. Jalón, B. R. Manzano, A. M. Rodríguez, J. V. Cuevas, G. Espino, M. A. Martínez, A. Massaguer, M. González-Bártulos, R. de Llorens, V. Moreno, J. Inorg. Biochem. 2012, 117, 171–188. c) M. Böge, C. Fowelin, P. Bednarski, J. Heck, Organometallics 2015, 34, 1507−1521.

15 (a) S. Krug, P. Michl, Minerva Gastroenterol. Dietol. 2012, 58, 427–443. (b) L. Rahib, B. D. Smith, R. Aizenberg, A. B. Rosenzweig, J. M. Fleshman, L. M. Matrisian, Cancer Res. 2014, 74, 2913–2921

16 I. Garrido-Laguna, M. Hidalgo, Pancreatic Nat. Rev. Clin. Oncol. 2015, 12, 319–334.

17 C. G. Hartinger, M. Groessl, S. M. Meier, A. Casini, P. J. Dyson, Chem. Soc. Rev. 2013, 42, 6186-6199.

18 a) A. Casini, C. Gabbiani, G. Mastrobuoni, L. Messori, G. Moneti, G. Pieraccini, ChemMedChem 2006, 1, 413–417. b) A. Casini, A. Guerri, C. Gabbiani, L. Messori, J. Inorg. Biochem. 2008, 102, 995–1006.

19 X. Jiang, X. Wang, Annu. Rev. Biochem. 2004, 73, 87–106.

20 H. A. McKenzie, F. H. White, Adv. Protein Chem. 1991, 41, 173–315.

21 G. Agonigi, T. Riedel, M. P. Gay, L. Biancalana, E. Oñate, P. J. Dyson, G. Pampaloni, E. Păunescu, M. A. Esteruelas, F. Marchetti, Organometallics 2016, 35, 1046−1056.

22 The synthesis of **1** has been published during the revision process of the present article: L. K. Batchelor, E. Paunescu, M. Soudani, R. Scopelliti, P. J. Dyson, Inorg. Chem. 2017, 56, 9617-9633.

23 See for instance: a) R. Pettinari, F. Marchetti, A. Petrini, C. Pettinari, G. Lupidi, P. Smoleński, R. Scopelliti, T. Riedel, P. J. Dyson, Organometallics 2016, 35, 3734−3742. b) S. Seršen, J. Kljun, K. Kryeziu, R. Panchuk, B. Alte, W. Körner, P. Heffter, W. Berger, I. Turel, J. Med. Chem. 2015, 58, 3984-3996.

24 J. S. M. Samec, R. Grubbs, Chem. Eur. J. 2008, 2686-2692.

25 a) Z. Wang, H. Qian, S.-M. Yiu, J. Sun, G. Zhu, J. Inorg. Biochem. 2014, 131, 47-55. b) S. Grgurić-Sĭpka, I. Ivanović, G. Rakić, N. Todorović, N. Gligorijević, S. Radulović, V. B. Arion, B. K. Keppler, Z. Tešic, Eur. J. Med. Chem. 2010, 45, 1051-1058. c) R. Sáez, J. Lorenzo, M. J. Prieto, M. Font Bardia, T. Calvet, N. Omeñaca, M. Vilasecae, V. Moreno, J. Inorg. Biochem. 2014, 136, 1-12. d) C. M. Clavel, E. Paunescu, P. Nowak-Sliwinska, A. W. Griffioen, R. Scopelliti, P. J. Dyson, J. Med. Chem. 2014, 57, 3546-3558.

26 a) C. S. Allardyce, P. J. Dyson, D. J. Ellis, S. L. Heath, Chem. Commun. 2001, 1396-1397. b) R. E. Morris, R. E. Aird, P. del S. Murdoch, H. Chen, J. Cummings, N. D. Hughes, S. Parsons, A. Parkin, G. Boyd, D. I. Jodrell, P. J. Sadler, J. Med. Chem. 2001, 44, 3616-3621. c) C. A. Vock, C. Scolaro, A. D. Phillips, R. Scopelliti, G. Sava, P. J. Dyson, J. Med. Chem. 2006, 49, 5552-5561.

27 a) M. Kawatsura, F. Ata, S. Wada, S. Hayase, H. Uno, T. Itoh, Chem. Commun. 2007, 298-300. b) B. Sundaraju, M. Achard, B. Demerseman, L. Toupet, G. V. M. Sharma, C. Bruneau, Angew. Chem. Int. Ed. 2010, 49, 2782-2785.

28 A. Bergamo, G. Sava, Dalton Trans. 2011, 40, 7817-7823.

29 The analysis of the CV response, with scan rates ranging between 0.020 and 1.00 $V \cdot s^{-1}$, confirmed the electrochemical reversibility: peak-to-peak separation approached the theoretical value of 59 mV at low scan rates, while $(I_p)_{ox}/v^{1/2}$, $(E_p)_{ox}$ and $(I_p)_{ox}/(I_p)_{red}$ remained almost unchanged during the scan rate.

30 a) F. Marchetti, C. Pettinari, A. Cerquetella, A. Cingolani, R. Pettinari, M. Monari, R. Wanke, M. L. Kuznetsov, A. J. L. Pombeiro, Inorg. Chem. 2009, 48, 6096–6108 (R = Ph, $E°'_{Ru2+/Ru3+}$ = +1.14 V vs. SCE in MeCN). b) P. D. Harvey, S. Tasan, C. P. Gros, C. H. Devillers, P. Richard, P. Le Gendre, E. Bodio, Organometallics 2015, 34, 1218–1227 [R = 4-C_6H_4COO(2,5-dioxopyrrolidin-1-yl), $E°'_{Ru2+/Ru3+}$ = +1.16 V vs. SCE in CH_2Cl_2]. c) P. D. Smith, A. H. Wright, J. Organomet. Chem. 1998, 559, 141–147 (R = $CH_2CH_2CH_2Ph$, $E°'_{Ru2+/Ru3+}$ = +1.25 V vs. SCE in CH_2Cl_2).

31 a) R. Bhalla, C. J. Boxwell, S. B. Duckett, P. J. Dyson, D. G. Humphrey, J. W. Steed, P. Suman, Organometallics 2002, 21, 924-928. b) F. Estevan, P. Lahuerta, J. Latorre, A. Sanchez, C. Sieiro, Polyhedron 1987, 6, 473-478.

32 J. C. Gray, A. Habtemariam, M. Winnig, W. Meyerhof, P. J. Sadler, J. Biol. Inorg. Chem. 2008, 13, 1111–1120.

33 G. Cynkowska, T. Cynkowski, A. A. Al-Ghananeem, H. Guo, P. Ashton, P. A. Crooks, Bioorg. Med. Chem. Lett. 2005, 15, 3524–3527.

34 (a) S. M. Meier, M. S. Novak, W. Kandioller, M. A. Jakupec, A. Roller, B. K. Keppler, C. G. Hartinger, Dalton Trans. 2014, 43, 9851–9855. (b) A. Casini, G. Mastrobuoni, W. H. Ang, C. Gabbiani, G. Pieraccini, G. Moneti, P. J. Dyson, L. Messori, ChemMedChem 2007, 2, 631-635.

35 M. A. Bennett, A. K. Smith, J. Chem. Soc., Dalton Trans. 1974, 233-241.

36 W. Willker, D. Leibfritz, R. Kerssebaum, W. Bermel, Magn. Reson. Chem. 1993, 31, 287-292.

37 a) A. Jutand, Eur. J. Inorg. Chem. 2003, 2017-2040. b) W. J. Geary, Coord. Chem. Rev. 1971, 7, 81-122.

38 V. Bonuccelli, T. Funaioli, P. Leoni, F. Marchetti, L. Marchetti, M. Pasquali, Dalton Trans. 2016, 45, 6878-6892.

39 M. Krejčik, M. Daněk, F. J. Hartl, Electroanal. Chem. 1991, 317, 179-187.

40 G. M. Sheldrick, SADABS, Program for empirical absorption correction, University of Göttingen, Germany (1996).

41 G. M. Sheldrick, SHELX97, Program for crystal structure determination, University of Göttingen, Germany (1997).